

AFRPL-TR-80-30

(2) ~~LEVEL~~

MULTICOLOR INVERSION DIAGNOSTIC FOR TACTICAL
MOTOR PLUMES

INTERIM REPORT

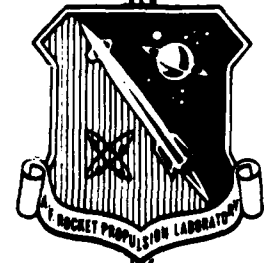
THE AEROSPACE CORPORATION
EL SEGUNDO, CALIFORNIA 90245

AUTHOR: STEPHEN J. YOUNG

MAY 1980

*Approved for Public Release
Distribution Unlimited*

Prepared for:
AIR FORCE ROCKET PROPULSION LABORATORY
DIRECTOR OF SCIENCE AND TECHNOLOGY
AIR FORCE SYSTEMS COMMAND
EDWARDS AFB, CALIFORNIA 93523



DTIC
S
MAY 8 1980
A


DDC FILE COPY

ADA083904

FOREWORD


This report was submitted by The Aerospace Corporation, P.O. Box 92957, Los Angeles, California, 90009, under Procurement Directive AFRPL/SAMSO 80-4, Job Order No. 573010CU with the Air Force Rocket Propulsion Laboratory, Edwards AFB, CA 93523.

This report has been reviewed by the Technical Information Office (STINFO)/TSPR and is releasable to the National Technical Information Service (NTIS). At NTIS it will be available to the general public, including foreign nations. This technical report has been reviewed and is approved for publication; it is unclassified and suitable for general public release.


T. DWAYNE MCCAY
Research Physical Scientist/
Project Manager


DR DAVID M. MANN
Chief, Plume Technology Office

FOR THE COMMANDER


EUGENE G. HABERMAN
Chief, Propulsion Analysis Division

UNCLASSIFIED

SECURITY CLASSIFICATION OF THIS PAGE (When Data Entered)

19 REPORT DOCUMENTATION PAGE		READ INSTRUCTIONS BEFORE COMPLETING FORM	
1. REPORT NUMBER	2. GOVT ACCESSION NO.	3. RECIPIENT'S CATALOG NUMBER	
(18) AFRPL-TR-80-30	AD-A083 904		
4. TITLE (and Subtitle)	5. TYPE OF REPORT & PERIOD COVERED	6. PERFORMING ORG. REPORT NUMBER	
(6) MULTICOLOR INVERSION DIAGNOSTIC FOR TACTICAL MOTOR PLUMES.	(9) Interim Final rpt.	(14) TR-0080(5623)-1	
7. AUTHOR(s)	8. CONTRACT OR GRANT NUMBER(s)		
(10) Stephen J. Young	(15) F04701-79-C-0080		
9. PERFORMING ORGANIZATION NAME AND ADDRESS	10. PROGRAM ELEMENT, PROJECT, TASK AREA & WORK UNIT NUMBERS		
The Aerospace Corporation El Segundo, Calif. 90245			
11. CONTROLLING OFFICE NAME AND ADDRESS	12. REPORT DATE	13. NUMBER OF PAGES	
Air Force Rocket Propulsion Laboratory Edwards Air Force Base, Calif. 93523	(11) May 1980	98	
14. MONITORING AGENCY NAME & ADDRESS (if different from Controlling Office)	15. SECURITY CLASS. (of this report)	15a. DECLASSIFICATION/DOWNGRADING SCHEDULE	
Space Division Air Force Systems Command Los Angeles, Calif. 90009 (12) 93	Unclassified		
16. DISTRIBUTION STATEMENT (of this Report)			
Approved for public release; distribution unlimited (16) 5750			
17. DISTRIBUTION STATEMENT (of the abstract entered in Block 20, if different from Report)			
(17) 10			
18. SUPPLEMENTARY NOTES			
19. KEY WORDS (Continue on reverse side if necessary and identify by block number)			
Rocket Plume Radiation Temperature Retrieval Concentration Retrieval Inversion Methods			
20. ABSTRACT (Continue on reverse side if necessary and identify by block number)			
A theoretical and analytical analysis is presented on the application of multispectral emission/absorption inversion to the retrieval of temperature and concentration profiles of tactical rocket motor plumes. Consideration is given to both monochromatic and band model spectral scales. A main conclusion drawn from the analysis is that application in the infrared on either the monochromatic or wide band spectral scale cannot yield adequate inversions for small plumes with mild temperature gradients such as those			

DD FORM 1473
(FACSIMILE)

UNCLASSIFIED

SECURITY CLASSIFICATION OF THIS PAGE (When Data Entered)

009500

4/3

UNCLASSIFIED

SECURITY CLASSIFICATION OF THIS PAGE(When Data Entered)

18. KEY WORDS (Continued)

20. ABSTRACT (Continued)

encountered for tactical rocket motor. Even under the most ideal circumstances, temperature and concentration errors up to 30% are encountered. The failing of the method is due to the lack of spatial resolution inherent in the inversion weighting functions.

In monochromatic atomic line application, the weighting functions are narrow enough to yield adequate spatial resolution and thus good inversion results. Here, however, complications concerning experimental spectral resolution (0.004 Å required at 6000 Å), chemical reactivity (up to 30% mole fraction sodium required) and the inability to retrieve concentration profiles render the method not immediately applicable.

Accession For	
NTIS	✓
DDI	
Unrecovered	
Justified	
By	
District	
Approved	
Dist.	RECEIVED
A	

UNCLASSIFIED

SECURITY CLASSIFICATION OF THIS PAGE(When Data Entered)

TABLE OF CONTENTS

1.	INTRODUCTION	1
2.	MULTICOLOR INVERSION THEORY	3
	2.1 Review	3
	2.2 Inversion Weighting Function	5
	2.3 Application to Atmospheric Sounding	10
	2.4 Industrial Furnace Application	12
	2.5 Monochromatic Formulation	13
	2.6 Inversion Procedure	16
3.	BAND MODEL APPLICATION	21
	3.1 Band Model Formulation	21
	3.2 Selection of Optimum Spectra Regions	24
	3.2.1 Species Overlap	24
	3.2.2 Weighting Function	30
	3.3 Test Inversions	31
	3.3.1 Temperature Variation Analysis	42
	3.3.2 Size Variation Analysis	56
4.	MONOCHROMATIC APPLICATION	67
	4.1 Monochromatic Weighting Functions	67
	4.2 Application to Molecular Lines	71
	4.3 Application to Atomic Lines	76
	4.4 Integrated Line Treatment for Atomic Lines	81
5.	SUMMARY AND CONCLUSIONS	85

LIST OF FIGURES

1.	Optical path geometry	7
2.	Weighting functions for atmospheric temperature sounding . .	11
3.	Temperature profile for furnace inversion application	14
4.	Weighting functions for furnace inversion application	14
5.	Radial pTc profiles for spectral overlap analysis	25
6.	H ₂ O and CO ₂ emission spectra near 2.7 μ m	26
7.	CO ₂ and CO emission spectra near 4.5 μ m	27
8.	CO ₂ , CO and H ₂ O emission spectra near 6 μ m	28
9.	Radial pTc profiles for basic BATES model plume	32
10.	Weighting functions and peak distributions for BATES model plume in CO ₂ 4.3- μ m red wing	33
11.	Weighting functions and peak distributions for BATES model plume in CO 4.6- μ m red wing	34
12.	Weighting functions and peak distributions for BATES model plume in H ₂ O 6.3- μ m red wing	36
13.	Temperature inversion results for BATES model plume	40
14.	Concentration inversion results for BATES model plume	41
15.	Weighting functions for T ₀ = 2500 K and T _B = 2000 K	44
16.	Weighting functions for T ₀ = 2500 K and T _B = 1500 K	45
17.	Weighting functions for T ₀ = 2500 K and T _B = 1000 K	46
18.	Weighting functions for T ₀ = 2500 K and T _B = 500 K	47

LIST OF FIGURES (Continued)

19.	Variation in weighting function with temperature gradient	48
20.	Variation in peak distribution with temperature gradient	50
21.	Convergence behavior for temperature and concentration residuals	53
22.	Temperature inversion results for four temperature gradient cases	54
23.	Variation of temperature inversion accuracy with temperature gradient	55
24.	Concentration inversion results for four temperature gradient cases	57
25.	Variation in weighting function with plume radius	59
26.	Variation in weighting function half-width (FWHM) with plume radius	60
27.	Variation in peak distribution with plume radius	62
28.	Temperature inversion results for four plume radii	65
29.	Triangular temperature profile for monochromatic analysis	70
30.	Monochromatic weighting function for molecular infrared line	72
31.	Comparisons among band model, molecular line and atomic line weighting function	73
32.	Sodium line monochromatic weighting function that peaks at $s/R = 0.3$	78

LIST OF TABLES

1.	Band model parameter summary	23
2.	Emission/Absorption inversion data for BATES model plume	39
3.	Variation of weighting function half-width (FWHM) with temperature gradient	49
4.	Emission/Absorption inversion data for temperature gradient variation	51
5.	Variation of weighting function half-width (FWHM) with plume radius	61
6.	Emission/Absorption inversion data for plume radius variation	63
7.	Required and available line strengths for three molecular species	75
8.	Atomic sodium line data	77

1. INTRODUCTION

In order to assess the accuracy of plume flow-field code predictions, the Air Force Rocket Propulsion Laboratory has sponsored a series of experimental and analytical programs to infer radial pressure, temperature and concentration (pTc) profiles from nonintrusive measurements of plume emission and absorption (E/A) characteristics. The significant programs completed to date are the HAPRAP, ERASE and NERD programs. References to the results of these programs are given in Ref. 1. The principal approach of these three programs was the mathematical inversion of infrared E/A profiles measured transverse to the plume axis at a fixed axial station and for a fixed spectral bandpass in order to retrieve the radial pTc profiles at that station. The E/A profiles obtained during a transverse spatial scan of the plume comprise two known profiles from which two of the three unknown pTc profiles may be determined. Generally, c and T are determined with p assumed to be known. The procedure is discussed in detail in Ref. 1. Such a method whereby the requisite information needed to perform an inversion is obtained by performing measurements on many independent lines of sight through the plume is known as multiposition inversion. As discussed briefly in Ref. 1, however, the requisite information can (in principle) also be obtained by holding the observation line of sight fixed (instead of spectral bandpass) and scanning in wavelength (rather than position). This approach is known as multicolor or multispectral inversion.

1. S. J. Young, Inversion of Plume Radiance and Absorptance Data for Temperature and Concentration, AFRPL-TR-78-60, Air Force Rocket Propulsion Laboratory, Edwards Air Force Base, California, 29 September 1978.

This report documents the results of the first phase of study on an overall project to develop a multicolor plume flow-field diagnostic for tactical rocket motors with light particle loading. The first phase concerned the formulation of an inversion scheme for the gas-only case (i. e., no particle loading). No further mention of particles will be made here. The work described here is in support of an in-house AFRPL experimental program that performs measurements on propellants in specially-designed motors mounted on an extremely accurate thrust stand. The acronym BATES (Ballistic Test and Evaluation System) will be used in this report to refer to this program and to the motors being examined in the program.

The general principles of multicolor inversion are discussed in Section 2. The central concept introduced in this section is the inversion "weighting function." The conditions that this function must satisfy in order that a successful inversion can be effected are considered. Also, the actual inversion algorithm for error-free data is derived. It is an extension of the Smith-Chahine method. In Section 3, the general principles are applied in the infrared using moderate resolution band model techniques. In Section 4, a high-resolution application is considered. A summary and conclusions discussion is presented in Section 5.

The general conclusion drawn from this report is that multispectral inversion whether on a band model or monochromatic spectral scale is not a viable diagnostic for motors as small as and with as mild temperature gradients as those encountered in BATES-type motor plumes.

2. MULTICOLOR INVERSION THEORY

2.1 Review

The bulk of the literature concerning multicolor inversion deals with its application to atmospheric sounding. Rodgers ⁽²⁾ has reviewed this field extensively. Although the study of meteorological applications is indispensable to an overall insight into the nature of multispectral inversion, most of the methods considered are not directly applicable to high-temperature gas problems. The primary difference between meteorological and combustion problems is the degree of temperature variation along the optical line of sight. In the former, the temperature gradients and extremes of variation are small enough that the mathematical inversion can be well approximated as a linear problem. In the latter, the gradients are too large for this approximation to be valid, and the general nonlinear problem has to be considered. It is the linear inversion problem that has received the most attention. For a "nearly-linear" problem, Wang and Goulard ⁽³⁾ and others have considered an initial linear inversion followed by iterative corrections to account for the nonlinear aspects of the problem.

Rodgers ⁽²⁾ and Wang ⁽⁴⁾ also review some nonlinear, iterative multispectral inversion methods that have been applied to various problems. Of

-
2. C. D. Rodgers, "Retrieval of Atmospheric Temperature and Composition from Remote Measurements of Thermal Radiation," *Rev. Geophys. Space Phys.* 14, 609-624 (1976).
 3. J. Y. Wang and R. Goulard, "Numerical Solutions in Remote Sensing," *Appl. Opt.* 14, 862-871 (1975).
 4. J. Y. Wang, Theory and Applications of Inversion Techniques: A Review, AAES 70-6, Purdue University, Lafayette, Indiana, September 1970.

these, the related method of Smith ⁽⁵⁾ and Chahine ⁽⁶⁾ appears to be most amenable to the present problem. This is reinforced by its successful application to a hot-gas (furnace) problem by Cutting and Stewart. ⁽⁷⁾ The Smith-Chahine approach is used in this present work and its formulation is given in Section 2.6.

The discussions presented so far have pertained to inversion techniques in which almost nothing is assumed to be known about the sought-for radial profiles. Methods of inversion in which some a priori assumptions on these profiles is made have been used by Simmons et al. ⁽⁸⁾ and Buchele. ⁽⁹⁾ In both of these works, the unknown profile is assumed to be given by some simple analytical function described in terms of a few adjustable parameters. The parameters are adjusted until the E/A profiles best match the observed E/A profiles. This method was not considered to be general enough for the present application.

-
5. W. L. Smith, "Iterative Solution of the Radiative Transfer Equation for the Temperature and Absorbing Gas Profile of an Atmosphere," Appl. Opt. 9, 1993-1999 (1970).
 6. M. T. Chahine, "Determination of the Temperature Profile in an Atmosphere from its Outgoing Radiance," J. Opt. Soc. Amer. 58, 1634-1637 (1968).
 7. R. D. Cutting and I. McC. Stewart, "Furnace Temperature Profiles: Measurement by Spectroscopic Methods," Appl. Opt. 14, 2707-2711 (1975).
 8. F. S. Simmons, H. Y. Yamada and C. B. Blake, Measurement of Temperature Profiles in Hot Gases by Emission-Absorption Spectroscopy, NASA CR-72491, NASA Lewis Research Center, Cleveland, Ohio, April 1969.
 9. D. R. Buchele, Computer Program for Calculation of a Gas Temperature Profile by Infrared Emission-Absorption Spectroscopy, NASA TM-73848, NASA Lewis Research Center, Cleveland, Ohio, December 1977.

The Phillips-Twomey ^(10,11) inversion method has been used by Krakow ⁽¹²⁾ for multispectral inversion in high-temperature gas problems. Generally, this method is applied to linear inversion problems, but it has been applied in an iterative fashion to nonlinear multiposition inversion problems ⁽¹⁾ and there is no intrinsic problem in adapting this method to the multispectral problem. In application, however, this method has one serious fault. The inversion requires the selection of two smoothing parameters. These parameters are not defined a priori and must be found empirically. The search for the proper parameters is quite time consuming.

2.2 Inversion Weighting Function

Ultimately, we will be concerned with inverting spectral profiles of emission and absorption obtained for a single line of sight through a plume (generally through a full diameter) in order to retrieve the spatial temperature and concentration profile along the line of sight. In order to present the underlying principle of the method, however, we can assume that the concentration profile is known. As suggested in the introduction, we also assume that the pressure profile is known. We consider, then, an inversion for temperature alone. In actuality, this situation obtains for all prior ap-

-
10. D. L. Phillips, "A Technique for the Numerical Solution of Certain Integral Equations of the First Kind," J. Assoc. Comp. Mach. 9, 84-97 (1962).
 11. S. Twomey, "On the Numerical Solution of Fredholm Integral Equations of the First Kind by the Inversion of the Linear System Produced by Quadrature," J. Assoc. Comp. Mach. 10, 97-101 (1963).
 12. B. Krakow, "Spectroscopic Temperature Profile Measurements in Inhomogeneous Hot Gases," Appl. Opt. 5, 201-210 (1965).

plications of this method (Sections 2.3 and 2.4) and the inversion for both T and c (Section 2.6) is an extended application of the method.

The general form of the radiative transfer equation for the radiation emitted in the -s direction from a line of sight through a hot gas sample lying between $s = 0$ and $s = L$ (See Fig. 1) is

$$N(\lambda) = \int_0^L B(\lambda, s) g(\lambda, s) ds \quad (1)$$

where $N(\lambda)$ is the radiant emission measured at wavelength λ , $B(\lambda, T)$ is the Planck radiation function evaluated at temperature $T(s)$ and λ , $T(s)$ is the line-of-sight temperature profile, and $g(\lambda, s)$ is a weighting function. Equation (1) is quite general and applies on any spectral scale if N and g are defined appropriately. For monochromatic applications, $N(\lambda)$ is the spectral radiance at λ and

$$g(\lambda, s) = \frac{-d\tau(\lambda, s)}{ds} \quad (2)$$

where $\tau(\lambda, s)$ is the spectral transmittance between $s = 0$ and s at wavelength λ . The next scale of spectral resolution is that of spectral line widths. In this case, $N(\lambda)$ is the integrated spectral radiance of an isolated line centered on λ and

$$g(\lambda, s) = \frac{dW(\lambda, s)}{ds} \quad (3)$$

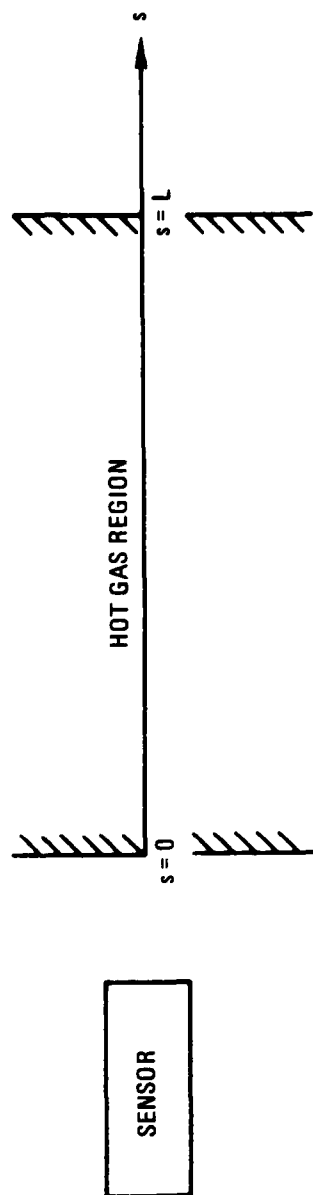


Fig. 1. Optical path geometry.

where $W(\lambda, s)$ is the equivalent width (integrated absorptance) of the line for the path segment $s = 0$ to s . The spectral scale of band model application is wide enough to include many tens or hundreds of individual lines in the resolution element $\Delta\lambda$. In this case, $N(\lambda)$ is the mean spectral radiance in $\Delta\lambda$ and

$$g(\lambda, s) = - \frac{d\bar{T}(\lambda, s)}{ds} \quad (4)$$

where $\bar{T}(\lambda, s)$ is the mean transmittance between $s = 0$ and s in the bandpass $\Delta\lambda$ centered on λ . All three of these forms will be considered in subsequent developments.

On any spectral scale, the goal of inversion is to obtain the function $B(\lambda, s)$ from measurements of $N(\lambda)$. When $B(\lambda, s)$ is known, the Planck equation can be inverted for temperature by

$$T(\lambda, s) = \frac{c_2}{\lambda \ln \left[1 + \frac{\lambda^5}{c_1} B(\lambda, s) \right]} \quad (5)$$

where

$$c_1 = 1.191 \times 10^4 \frac{W}{\text{cm}^2 \text{-sr-}\mu\text{m}} \mu\text{m}^5$$

$$c_2 = 1.4388 \times 10^4 \mu\text{m-K}.$$

In principle, the result for T should not depend on λ .

In order to effect a successful inversion by any spectral means, the weighting function must satisfy two fundamental conditions. First, it must be a sharply peaked function with peak position $0 \leq s_p \leq L$. Some estimates of how sharply peaked it must be for the present application to plumes are made in Section 2.4. Second, the position of the peak must be a function of λ and must traverse at least the entire interval from 0 to L as λ passes between the upper and lower experimental spectral bounds. The reason for these two conditions is made more clear if we consider an ideal inversion in which the weighting function is infinitely sharp. Then, over the infinitely small region Δs about the position s_p where the function peaks, $B(\lambda, s)$ can be considered as constant with the value $B(\lambda, s_p)$. Taking $B(\lambda, s_p)$ outside the integral sign in Eq. (1) and performing the integration (for the monochromatic case, for example), we get

$$N(\lambda) = B(\lambda, s_p) \left[1 - \tau(\lambda, L) \right] \quad (6)$$

where $\tau(\lambda, L)$ is the transmittance of the entire path and is presumed to be known. Thus, for a weighting function that peaks sharply at s_p for wavelength λ , the measurement of $N(\lambda)$ determines $B(\lambda, s)$ at that position, and thus the temperature at that position. For different λ , the position of the peak in the weighting function changes and thus different regions of the path may be probed. In order to probe the entire optical path, a set of λ must be selected such that the peak position varies over the entire path. Example illustrations of the form of the weighting functions for two previous applications in which

multicolor inversion has been successful are presented in the following two sections.

2.3 Application to Atmospheric Sounding

The most extensive literature on multicolor inversion pertains to its application to the meteorological sounding of the earth's atmosphere for temperature and concentration. In sounding for temperature, a space sensor measures the radiance in narrow (a few wavenumbers wide) spectral regions of, for example, the CO₂ 4.3- μ m or 15- μ m band. An altitude pressure profile and a constant CO₂ mixing ratio are assumed. The weighting function is⁽¹³⁾

$$-\frac{d\bar{\tau}(\lambda, s)}{ds} = b(\lambda) p(s) e^{-a(\lambda)p(s)} \quad (7)$$

where $p(s)$ is pressure and $a(\lambda)$ and $b(\lambda)$ are functions of λ only. The formation of a peak is caused by the approximately exponential increase of $p(s)$ with s . (The $+s$ axis is down into the atmosphere.) Thus, $p(s)$ is an increasing function while $e^{-a(\lambda)p(s)}$ is a decreasing function. The opposing effects of the two functions cause a peak to be formed at the position s where $p(s) = 1/a(\lambda)$. The form of the weighting function for this application is shown in Fig. 2. With the λ selection tabulated in the figure, the peaks of the weighting functions are distributed over pressure levels from 20 mb (altitude ~ 25 km) to 100 mb (sea level). Consequently, temperature retrieval can be obtained over the same region. The widths of the weighting functions indicate that the spatial resolution of the retrieval profile would be about 2 km.

13. L. D. Kaplan, M. T. Chahine, J. Susskind, and J. E. Searl, "Spectral Band Passes for a High Precision Satellite Sounder," Appl. Opt. 16, 322-325 (1977).

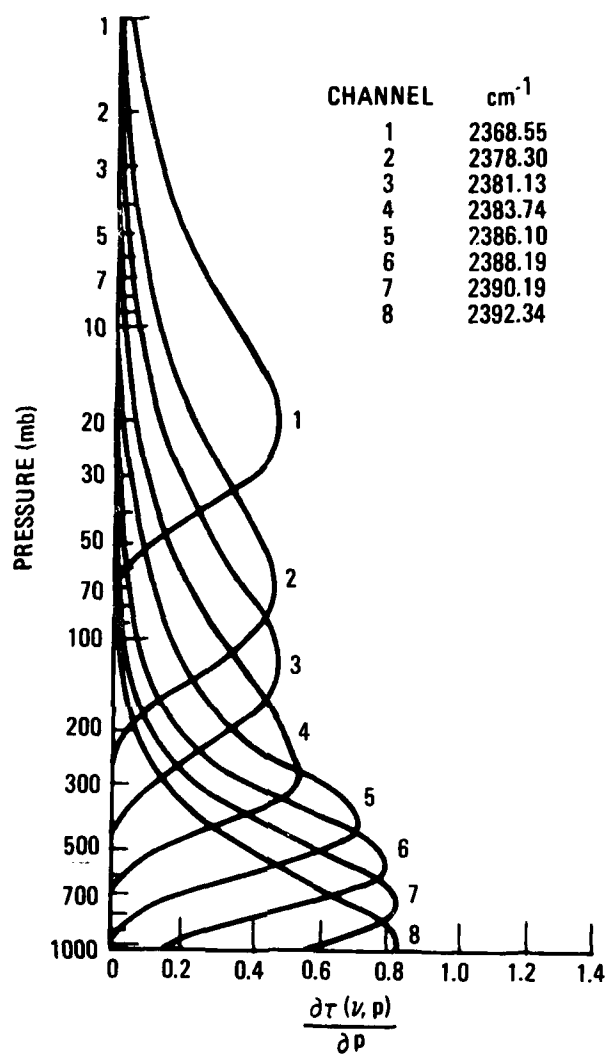


Fig. 2. Weighting functions for atmospheric temperature sounding. Spectral resolution is 2 cm^{-1} and spectral region is the $4.3\text{-}\mu\text{m}$ CO_2 red wing. From Kaplan et al. ⁽¹³⁾

2.4 Industrial Furnance Application

The second example is the retrieval of industrial furnace temperature profiles, (7) and is quite comparable to the plume application. In this case, the weighting function is (see Section 3.1).

$$\frac{-d \bar{T}(s)}{ds} = c(s) p(s) \bar{k}(s) y(s) \bar{T}(s) \quad (8)$$

where the product $c(s) p(s)$ is the partial pressure of active gas and $\bar{k}(s)$ is the band model absorption parameter. $y(s)$ is a complicated function whose only nature we need be concerned with at present is that it decreases with increasing s . In the atmospheric application, the peak in the weighting function was caused by the exponential variation of pressure along the path. In the furnace application (and to a large extent in the plume application), the pressure is constant along the path. The required formation of the peak is caused by a different effect -- namely, the variation of temperature along the path. In particular, the temperature profile must be such that the absorption band model parameter (which is temperature dependent) increases with s . Then the interplay of this increase and the decrease of $y(s)$ and $\bar{T}(s)$ with s can form a peak. In most spectral regions, \bar{k} increases with T . In this case a peak is formed in the weighting function only if the temperature increases with s . In both the furnace and plume application, this occurs only if the temperature is highest near the center of the system and falls to lower values at the boundaries.

The temperature profile used by Cutting and Stewart ⁽⁷⁾ in their furnace analysis is shown in Fig. 3 and the weighting functions for selected λ in the red wing of the CO_2 fundamental in Fig. 4. The λ 's were selected to give a nearly equal distribution of peaks between the furnace boundary and center. Because of the large widths of the weighting function peaks, a spatial resolution of only $\sim 1/5$ of the boundary-to-center distance is achievable. This resolution is, however, adequate to retrieve the temperature profile of Fig. 3 to a few percent.

Except for physical size, the furnace conditions are comparable to those encountered in tactical motor plumes. The furnace "diameter" is 10 m, while for plumes diameters of order 20 cm will be considered. However, an estimate of how narrow weighting functions must be in order to effect a reasonable inversion can be obtained from the furnace weighting functions. As a standard for future comparison, we note here that the function that peaks at a distance of 150 cm along the line of sight has a half width of 140 cm ($\Delta s_{1/2}/R = 0.28$ at $s/R = 0.3$ where $R = 500$ cm is the "radius" of the furnace).

2.5 Monochromatic Formulation

Both of the preceding applications were on a band model spectral scale although the reasons for peak formation were caused by different physical variations (i. e., pressure variation in one case and temperature variation in the other). In Section 4, consideration will be made of weighting

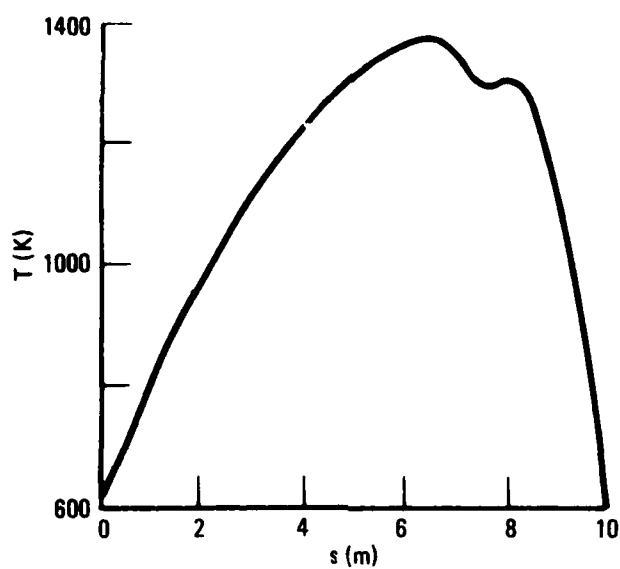


Fig. 3. Temperature profile for furnace inversion application. From Cutting and Stewart. ⁽⁷⁾

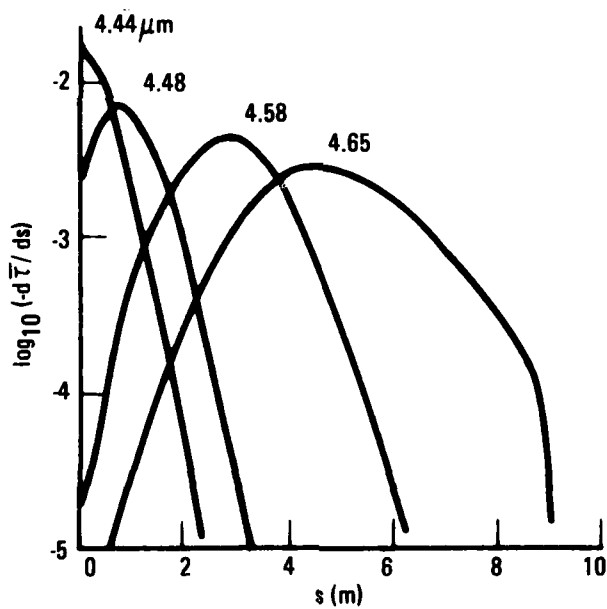


Fig. 4. Weighting functions for furnace inversion application. From Cutting and Stewart. ⁽⁷⁾

functions for monochromatic resolution, and it is convenient to show here how peaking results in this case. For the furnace or plume application, it is again the temperature variation, but the physical reasons for the rise and fall of the function are more immediately obvious than for the band model case. The spectral transmittance between $s = 0$ and general path position s is

$$\tau(\lambda, s) = \exp \left\{ - \int_0^s c(s') p(s') k(\lambda, s') ds' \right\} \quad (9)$$

where $c(s)$ is the mole fraction of active gas, $p(s)$ is the total gas pressure, and $k(\lambda, s)$ is the spectral absorption coefficient. From Eq. (2), the weighting function is

$$\frac{-d\tau(\lambda, s)}{ds} = c(s) p(s) k(\lambda, s) \tau(\lambda, s). \quad (10)$$

Consider an isolated Lorentz line for which the absorption coefficient is

$$k(\lambda, s) = \frac{S(s)}{\pi} \frac{\gamma(s)}{\nu^2 + \gamma^2(s)} \quad (11)$$

where $S(s)$ is the line strength, $\gamma(s)$ is the line width, and $\nu = 1/\lambda$ ($\nu = 0$ is the line center). In order to display the main features of the weighting function, assume $c(s)$, $p(s)$ and $\gamma(s)$ are slowly varying with s and approximate the temperature dependence of $S(s)$ by

$$S = \frac{S_0}{T} e^{-\theta/T} \quad (12)$$

where S_0 is an intrinsic line strength and θ is the lower energy level (expressed in temperature units) of the transition causing the line. Use of Eq. (11) and (12) in (10) yields

$$\frac{-d\tau(\lambda, s)}{ds} = \frac{C(\lambda)}{T(s)} e^{-\theta/T(s)} \tau(\lambda, s) \quad (13)$$

where

$$C(\lambda) = \frac{cp\gamma S_0}{\pi(\nu^2 + \gamma^2)} \quad (14)$$

The formation of a peak in Eq. (13) is caused by the opposing actions of the increase in $e^{-\theta/T(s)}$ with s [assuming $T(s)$ increases with s], and the decrease in transmittance to the boundary [i.e., $\tau(\lambda, s)$] as s increases. In order to obtain a sharp rise in the weighting function, θ should be large. The fastest rise occurs when θ is approximately twice the characteristic plume temperature. Thus, multicolor inversion can work only by looking at hot lines. In order to obtain a sharp fall-off, the product $cp\gamma S_0$ should be large. For fixed $cp\gamma$ this implies that one must look at lines with large intrinsic strength. It is shown in following analyses that the θ and S_0 conditions cannot be met with molecular lines, but can with atomic lines.

2.6 Inversion Procedure

The previous discussions concern the central issue in multispectral inversion, that is the shape of weighting functions, but do not indicate a method for actually producing and inversion. This procedure is formulated

here and is based on the iterative method of Smith ⁽⁵⁾ and Chahine. ⁽⁶⁾ The method is more general than previously used in that provisions are made for retrieving both temperature and concentration. The formulation is made within the context of band models, but the principle is easily extendable to other spectral scales. Also, the spectral variable $\nu = 1/\lambda$ is used in the formulation.

Consider a general optical path extended through a gas from position $s = 0$ to $s = L$. The radiance emerging from the path at $s = 0$ is

$$\bar{N}(\nu) = \int_0^L J(\nu, s)w(\nu, s)ds \quad (15)$$

and the absorptance of external radiation shown through the gas is

$$\bar{W}(\nu) = -\ln \bar{\tau}(\nu) = \int_0^L K(\nu, s)y(\nu, s)ds. \quad (16)$$

ν represents spectral position, and the bar over N and W indicate average values in a spectral interval $\Delta\nu$ centered on ν . In the present case, this $\Delta\nu$ is the spectral resolution of the band model parameters. The remaining variables are the same as used in Ref. 1 (see Section 3.1 also). Briefly J and K are the source and absorption functions, respectively, and w and y are functions defined by the band model formulation. The objective of inversion is to determine $J(\nu, s)$ and $K(\nu, s)$ given $\bar{N}(\nu)$ and $\bar{W}(\nu)$. From J and K , the temperature and concentration functions $T(\nu, s)$ and $c(\nu, s)$ can be obtained (see Ref. 1). Since T and c cannot physically depend on ν , weighted

averages are taken to define

$$T(s) = \frac{\int_{\nu} T(\nu, s) \bar{k}(\nu, s) w(\nu, s) d\nu}{\int_{\nu} \bar{k}(\nu, s) w(\nu, s) d\nu} \quad (17)$$

$$c(s) = \frac{\int_{\nu} c(\nu, s) \bar{k}(\nu, s) y(\nu, s) d\nu}{\int_{\nu} \bar{k}(\nu, s) y(\nu, s) d\nu} \quad (18)$$

where $\bar{k}(\nu, s)$ is the absorption band model parameter. This averaging procedure constitutes a smoothing aspect of the inversion should there be noise on the input profiles \bar{N} and \bar{W} .

The actual solution for J and K is an iterative process. A first guess to J and K is to assume that the optical path is uniform and to apply standard gas pyrometric methods. This procedure defines the functions J(ν) and K(ν) (independent of s) from which one gets T(ν) and c(ν) which when inserted into Eqs. (17) and (18) gives the first guess uniform profiles T and c.

Given the j^{th} guess to T(s) and c(s), one computes the following quantities using the band model radiation formulation

$$\begin{aligned} J_j(\nu, s) \\ K_j(\nu, s) \\ w_j(\nu, s) \end{aligned} \quad (19)$$

$$y_j(\nu, s)$$

$$\overline{N}_j(\nu, s)$$

$$W_j(\nu, s).$$

New source and emission functions are defined by the relaxation equations

$$J_{j+1}(\nu, s) = J_j(\nu, s) \frac{\overline{N}(\nu)}{\overline{N}_j(\nu)} \quad (20)$$

$$K_{j+1}(\nu, s) = K_j(\nu, s) \frac{\overline{W}(\nu)}{\overline{W}_j(\nu)}$$

where nonsubscripted \overline{N} and \overline{W} are the experimental data profiles. These new functions are inverted for $T_{j+1}(\nu, s)$ and $c_{j+1}(\nu, s)$ and used in Eqs. (17) and (18) to define the $j+1$ iteration on $T(s)$ and $c(s)$. The procedure is repeated until some criterion of convergence is met, and initiated, of course, with the first order uniform guesses T and c .

The relaxation equations [Eq. (20)] are derived from the transfer equations [Eqs. (15) and (16)] for the case of an optically thin, uniform optical path and should give near exact inversions for these conditions in one iteration.

The method derived here is essentially the standard Smith-Chahine iteration method except that the inversion for concentration is included. This more general formulation is not applicable to either the atmospheric or furnace discussed previously. In both cases, the absorptance through

the gas sample is so large that \bar{T} is immeasurably small. Thus, only one profile (the radiance profile) can be measured, and, consequently, only one profile (the temperature profile) can be retrieved. The concentration profile in these examples must be assumed to be known.

3. BAND MODEL APPLICATION

3.1 Band Model Formulation

The band model formulation used here is essentially that developed for the plume radiation code ATLES⁽¹⁴⁾ and the multiposition inversion code EMABIC.⁽¹⁾ The mean radiance and transmittance in a spectral interval $\Delta\nu$ containing many spectral lines are computed by

$$\bar{N} = - \int_0^L B(s) \frac{d\bar{\tau}(s)}{ds} ds \quad (21)$$

and

$$\bar{\tau} = \exp \left[- \int_0^L \frac{1}{\delta} \frac{d\bar{W}(s)}{ds} ds \right] \quad (22)$$

respectively. The transmittance and equivalent width derivatives are given by

$$\frac{d\bar{\tau}(s)}{ds} = - \bar{\tau}(s) \frac{1}{\delta} \frac{d\bar{W}(s)}{ds} \quad (23)$$

and

$$\frac{d\bar{W}(s)}{ds} = c(s)p(s) \bar{k}(s) y[x(s), \rho(s)] \quad (24)$$

respectively, where $y(x, \rho)$ is the equivalent width derivative function, $x(s)$ is a measure of optical depth, and ρ is a measure of local nonuniformity of the optical path. For greater detail, the reader is directed to Refs. 1

14. S. J. Young, Description and Use of the Plume Radiation Code ATLES, TR-0077(2753-04)-3, The Aerospace Corporation, El Segundo, California, 13 May 1977.

and 14 and the reference lists included therein. Only relatively mild temperature and concentration gradients are treated in the present application, and the derivative function appropriate to the traditional Curtis-Godson approximation is used exclusively. Also, since the present application concerns pressures near atmospheric, the Lorentz (pressure broadened) line profile is appropriate and used throughout.*

Band model parameters required for radiation calculation are also described in Ref. 14 and references cited therein. Table 1 contains a summary of information relevant to the parameters used here for H_2O , CO_2 and CO . Parameter sets with prefix N are obtained directly from the NASA handbook,⁽¹⁵⁾ those with prefix L are derived from the AFGL optical line compilation,⁽¹⁶⁾ and those with prefix C are a combination of

*A computer code MUSIC (Multispectral Inversion Code) has been written which includes other calculation options. The code and an informal user's manual have been delivered to AFRPL/PACP. Interested readers should contact that facility to inquire about the availability of the code.

15. C. B. Ludwig, W. Malkmus, J. E. Reardon, and J. A. L. Thompson, Handbook of Infrared Radiation from Combustion Gases, eds. R. Goulard and J. A. L. Thompson, NASA SP-3080, Marshall Space Flight Center, Huntsville, Ala., 1973.
16. R. A. McClatchey, W. S. Benedict, S. A. Clough, D. E. Burch, R. F. Calfe, K. Fox, L. S. Rothman and J. S. Garing, AFCRL Atmospheric Absorption Line Parameters Compilation, AFCRL-TR-73-006, Air Force Geophysics Laboratory, Hanscomb Air Force Base, Mass., 25 January 1973.

Table 1. Band Model Parameter Summary

Set No.	Name ⁽¹⁾	$\nu_1 \rightarrow \nu_2$ (cm ⁻¹) ⁽²⁾	ν_S (cm ⁻¹) ⁽³⁾	$\Delta\nu$ (cm ⁻¹) ⁽⁴⁾
1	CH ₂ O(2. 7)	2500 - 4500	25	25
2	NH ₂ O(6. 3)	1150 - 2500	25	25
3	CCO ₂ A(4. 3)	2000 - 2400	5	5
4	CCO ₂ B(4. 3)	2000 - 2415	5	25
5	CCO ₂ C(2. 7)	3100 - 3770	5	5
6	CCO ₂ D(2. 7)	3100 - 3785	5	25
7	NCO(4. 6)	1100 - 2350	25	~ 25
8	NHCl(3. 5)	1000 - 3225	variable	~ 25

- (1) Prefix letter indicates origin of data: N = NASA Tabulation;
C = Combined
- (2) Spectral region.
- (3) Spectral step size of data.
- (4) Spectral resolution of data.

Temperature range of data with prefix C is 100 - 3000K.

Temperature range of data with prefix N is 300 - 3000K.

parameters from the NASA handbook and parameters derived from the AFGL compilation. (17, 18)

3.2 Selection of Optimum Spectral Regions

Two conditions must obtain for a spectral region to be a candidate for multispectral inversion. First, the region must be spectrally clean, that is, the emission and absorption must arise from a single species. Second, the weighting functions in the region must have the proper peaking form and span the whole length of the optical path (for plumes, half the optical path).

3.2.1 Species Overlap

In order to investigate the first condition, emission spectra for CO_2 , H_2O and CO were generated in the 2- to 9- μm spectral region for the plume properties shown in Fig. 5. The emission spectra were generated with the band model parameter sets listed in Table 1 (with the 5 cm^{-1} spectral resolution option for the CO_2 fundamental at 4.3 μm). The Lorentz line shape and Curtis-Godson nonuniformity approximation options were employed. The results are plotted in Figs. 6-8. (Note that these spectra were generated for each species individually. The total radiance in any region of overlap is

-
17. S. J. Young, Band Model Parameters for the 2.7- μm Bands of H_2O and CO_2 in the 100-3000°K Temperature Range, TR-0076(6970)-4, The Aerospace Corporation, El Segundo, CA, 31 July 1975.
 18. S. J. Young, Band Model Parameters for the 4.3- μm Fundamental Band of CO_2 in the 100-3000°K Temperature Range, TR-0076(6754-03)-1, The Aerospace Corporation, El Segundo, CA, 19 February 1976.

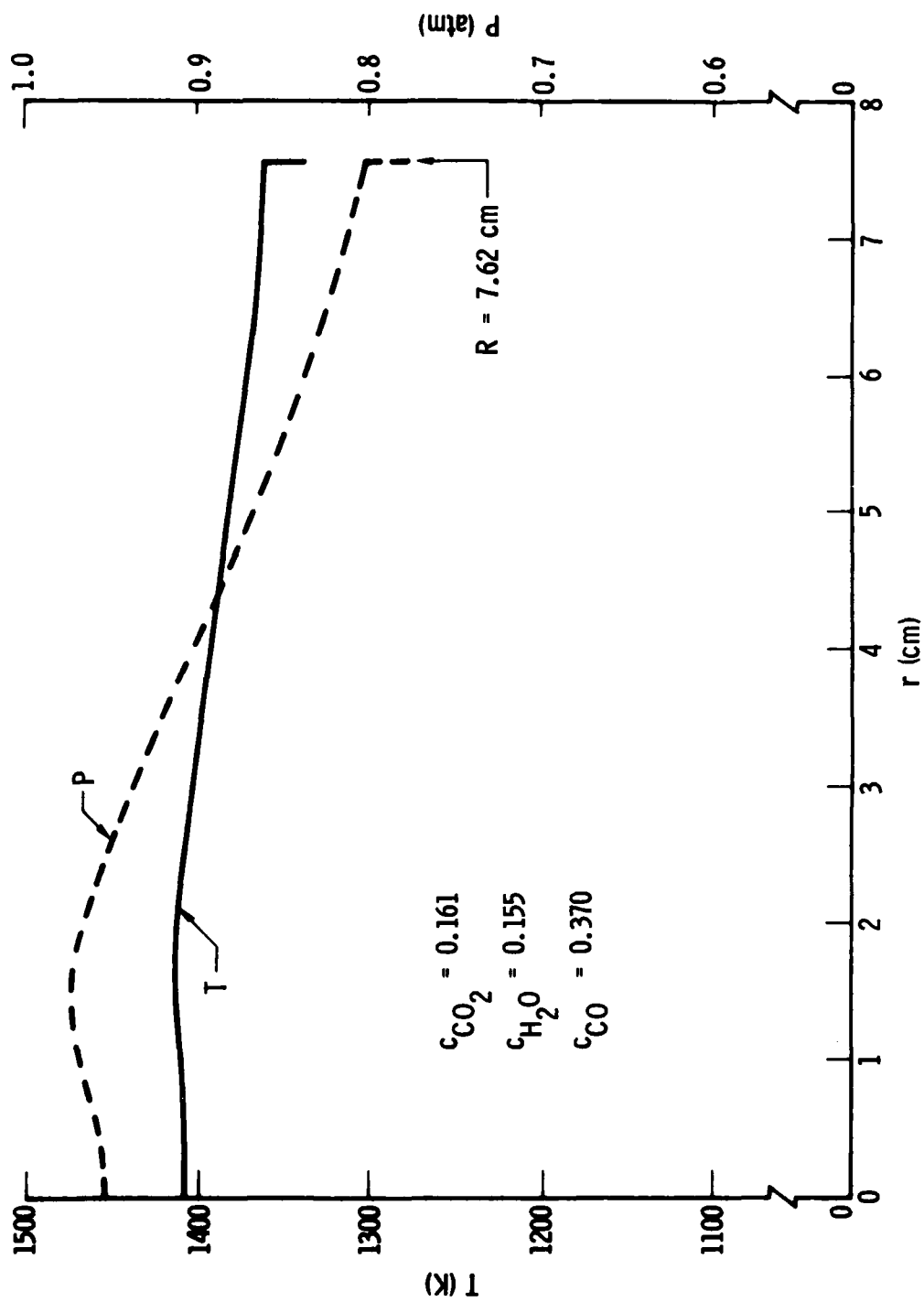


Fig. 5. Radial pTc profiles for spectral overlap analysis.

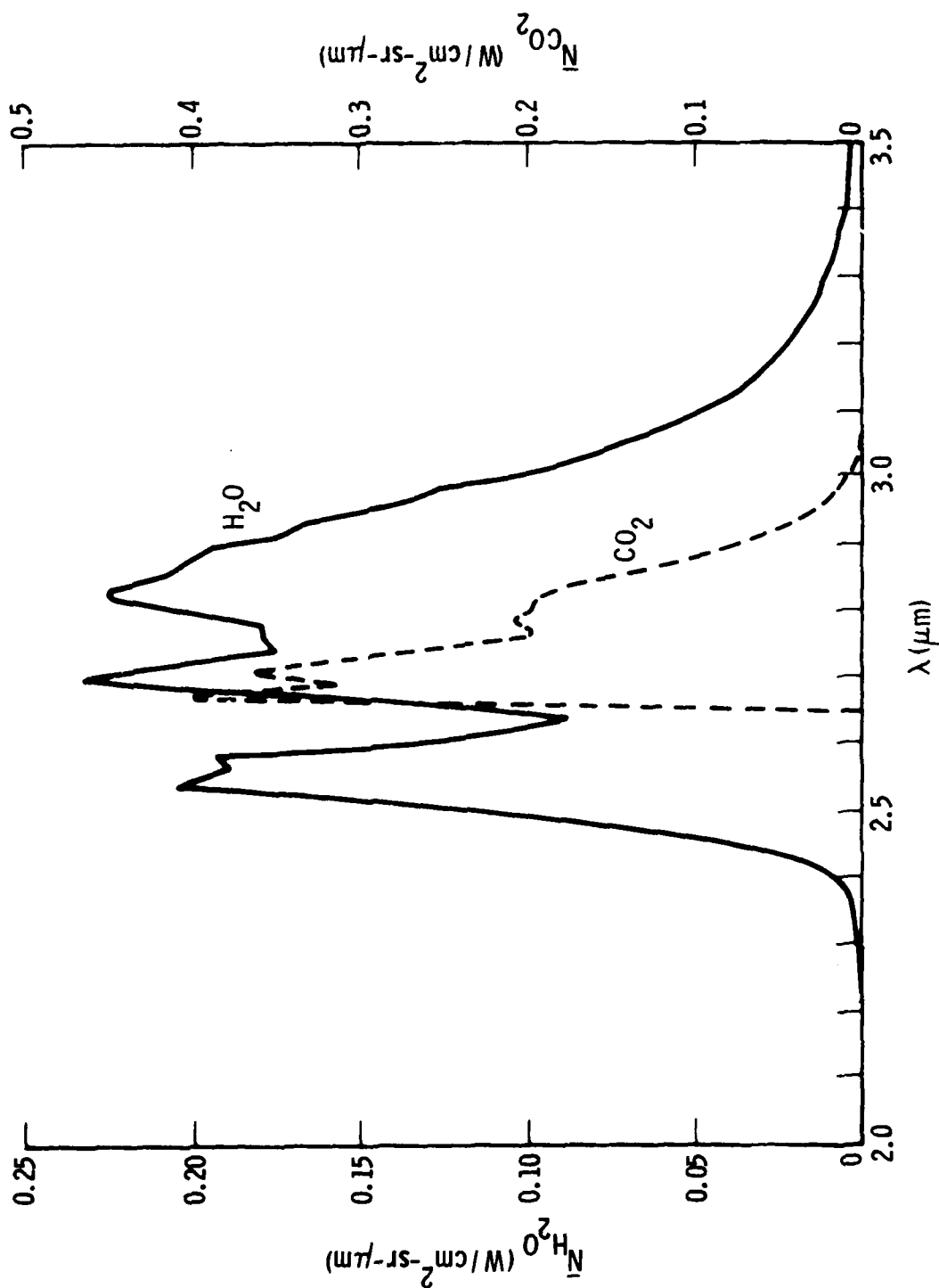


Fig. 6. H_2O and CO_2 emission spectra near $2.7 \mu m$.

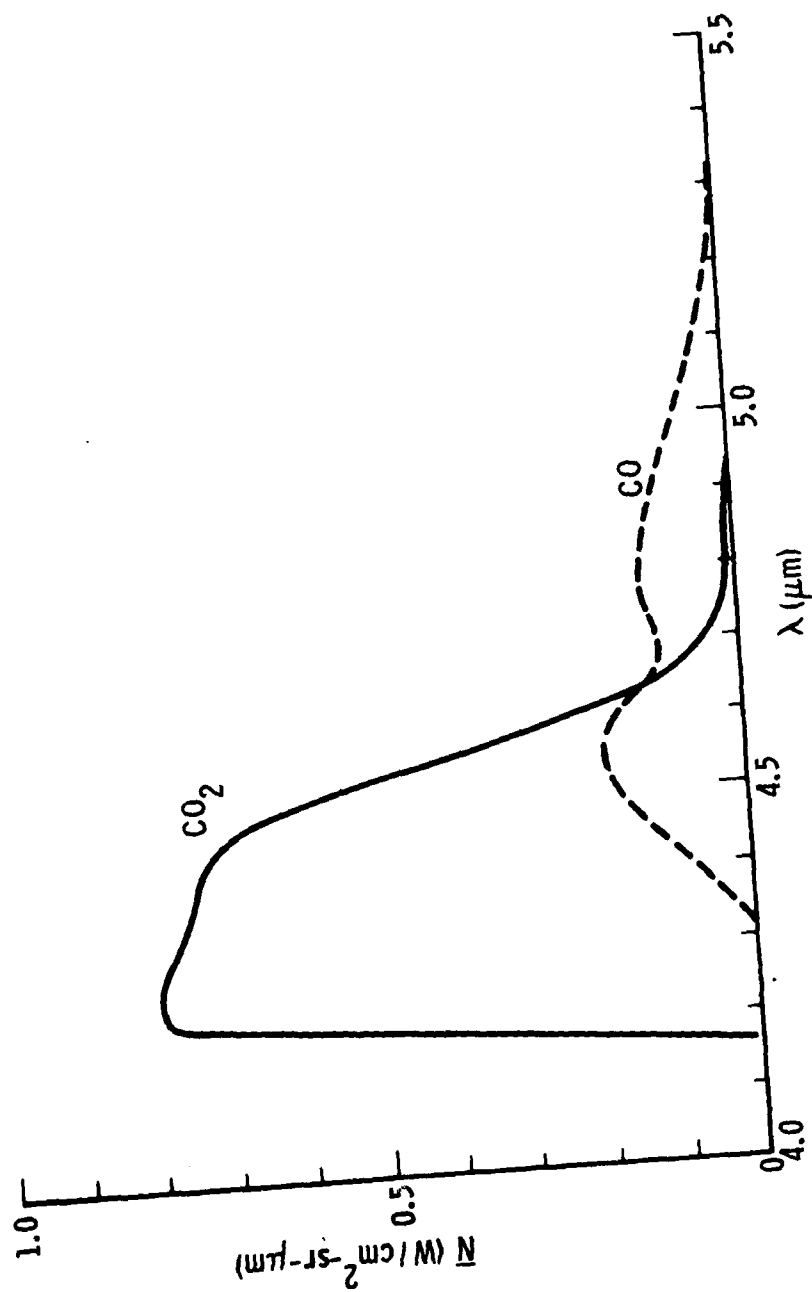


Fig. 7. CO₂ and CO emission spectra near 4.5 μm .

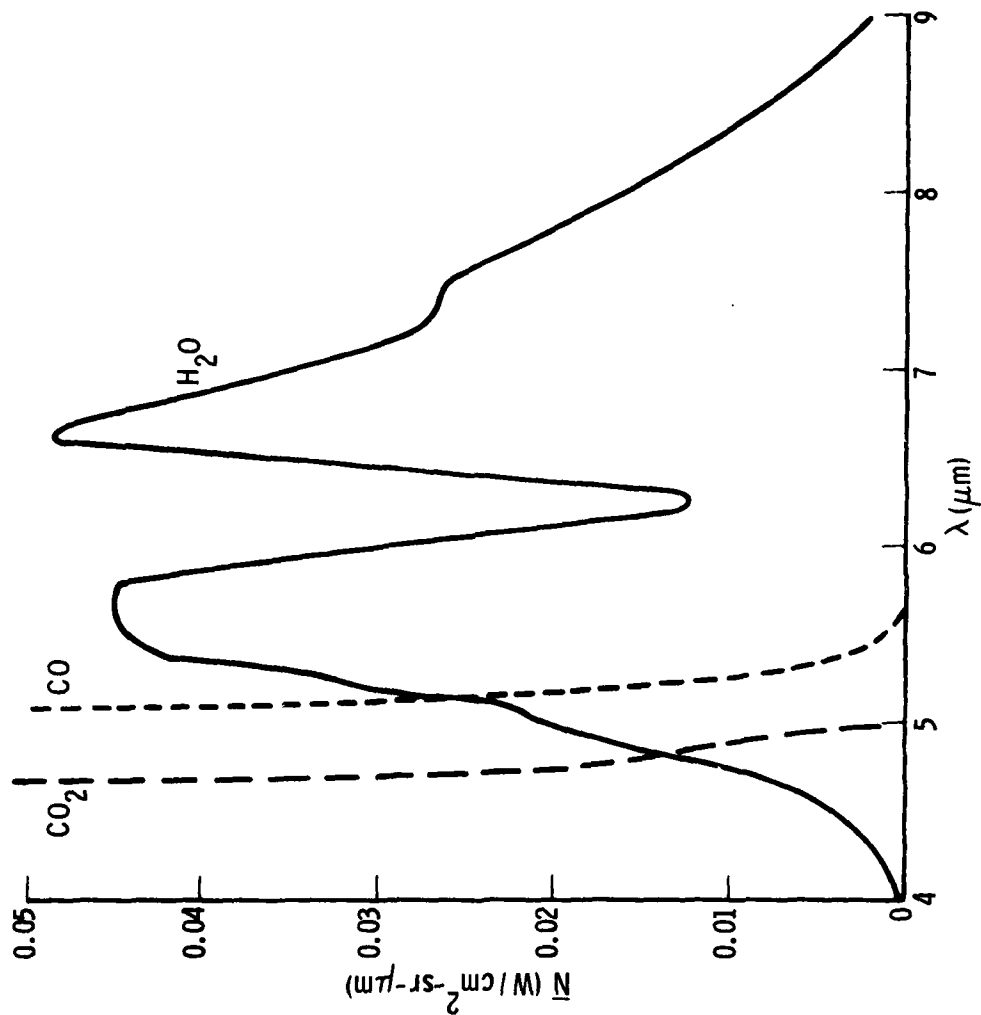


Fig. 8. CO_2 , CO and H_2O emission spectra near 6 μm .

not the sum of the radiances of the contributing species). The following conclusions can be drawn:

- (1) The only available spectral region for inversion with CO_2 as the emitting species is the fundamental band head region between 4.14 and 4.31 μm (Fig. 7). Beyond 4.31 μm , CO radiation seriously contaminates the CO_2 spectra. The 2.7- μm band of CO_2 is unavailable because it is entirely embedded in the 2.7- μm H_2O band (Fig. 6). In addition, not all of the allowed region around the fundamental band head is useful. Beyond $\lambda \sim 4.23 \mu\text{m}$, the source is essentially black and contains no information. Thus, the allowed region for CO_2 detection is only the very steeply rising region between 4.14 and 4.23 μm . Because of the narrowness of this region, an experimental resolution of $\sim 0.01 \mu\text{m}$ would be required for data acquisition.

The strong overlap between CO_2 and CO in this region, coupled with the strong CO emission, is a serious circumstance since it essentially eliminates the CO_2 red wing from consideration, and it is this region where multispectral inversion data is traditionally taken.

- (2) There are three regions of spectral cleanliness for H_2O observation: (a) the blue wing of the 2.7- μm band from ~ 2.3 to 2.64 μm (Fig. 6), (b) the red wing of the same band

- (3.1 to $\sim 3.5 \mu\text{m}$), and (c) the $6.3\text{-}\mu\text{m}$ band beyond $\lambda \sim 6 \mu\text{m}$ (Fig. 8). The center of the $2.7\text{-}\mu\text{m}$ band is eliminated by the $2.7\text{-}\mu\text{m}$ CO_2 band. Of these two regions in the $2.7\text{-}\mu\text{m}$ band, the blue wing is more sure to be free of CO_2 emission because it is below the CO_2 band head. The allowed region in the $6.3\text{-}\mu\text{m}$ band is limited on the low wavelength side by CO and CO_2 contamination.
- (3) The serious overlapping of the CO_2 and CO fundamental bands limits the available CO spectral region to lie beyond $\lambda \sim 5.0 \mu\text{m}$ (Fig. 6).

In summary, the spectral regions available after consideration of species overlap are:

- | | |
|--------------------------|--------------------------------------|
| (1) CO_2 | 4.14 to 4.23 μm |
| (2) H_2O | ~ 2.3 to 2.64 μm |
| | 3.10 to $\sim 3.5 \mu\text{m}$ |
| | ~ 6.0 to $\sim 6.9 \mu\text{m}$ |
| (3) CO | ~ 5.0 to $\sim 5.3 \mu\text{m}$ |

3.2.2 Weighting Functions

Even in a spectral region where only a single plume species is radiating, there is no guarantee that data taken in this region can be used to effect an inversion. Data taken within the spectral region must have a high enough degree of "independence" between them so as not to yield an indeterminate or trivial solution. In other words, the weighting functions must display a peak structure. Weighting functions were generated for a

model plume in the five clean regions just identified. Calculations were also carried out for the red wing of the CO_2 fundamental even though the species overlap consideration eliminated this region. The plume model is shown in Fig. 9 and is a crude estimate of what the full scale BATES motor might produce when a low visibility propellant is used.

Weighting function plots are shown in Figs. 10-12 for CO_2 (4.3- μm red wing), CO (4.6- μm red wing) and H_2O (6.3- μm red wing), respectively. In each of these figures, part (a) shows $-\bar{dT}/ds$ versus s for various wavelengths. Part (b) is a plot of where the weighting function peaks as a function of λ . Plots are not shown for either the blue or red wing of the 2.7- μm H_2O band or the blue wing of the 4.3- μm CO_2 band. For H_2O , a peak structure is formed, but the degree of absorption (as measured by the rate at which $y(s)$ decreases with s) is so slight that the position of the peak never moves closer than ~ 7 cm to the plume boundary. That is, the outer 7 cm of the plume cannot be probed. In the 4.3- μm CO_2 blue wing, the weighting functions decrease monotonically from $s = 0$ so that no peaking (except at $s = 0$) occurs. This monotonic decrease occurs because \bar{k} decreases with temperature in this region.

3.3 Test Inversions

A common feature of the weighting functions for the three spectral regions in which the required peak structure occurs (Figs. 10-12) is the large widths of the peaks. This excessive width leads to poor spatial resolution. The consequence of poor resolution is evident in the following

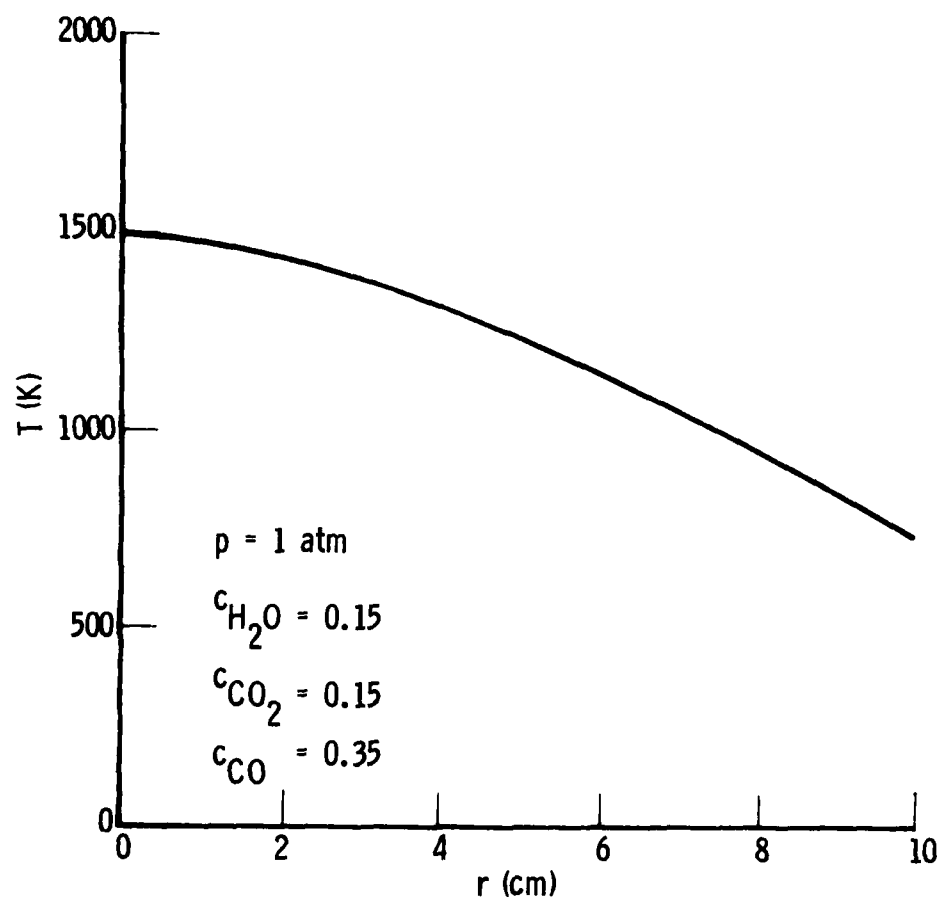


Fig. 9. Radial pTc profiles for basic BATES model plume.

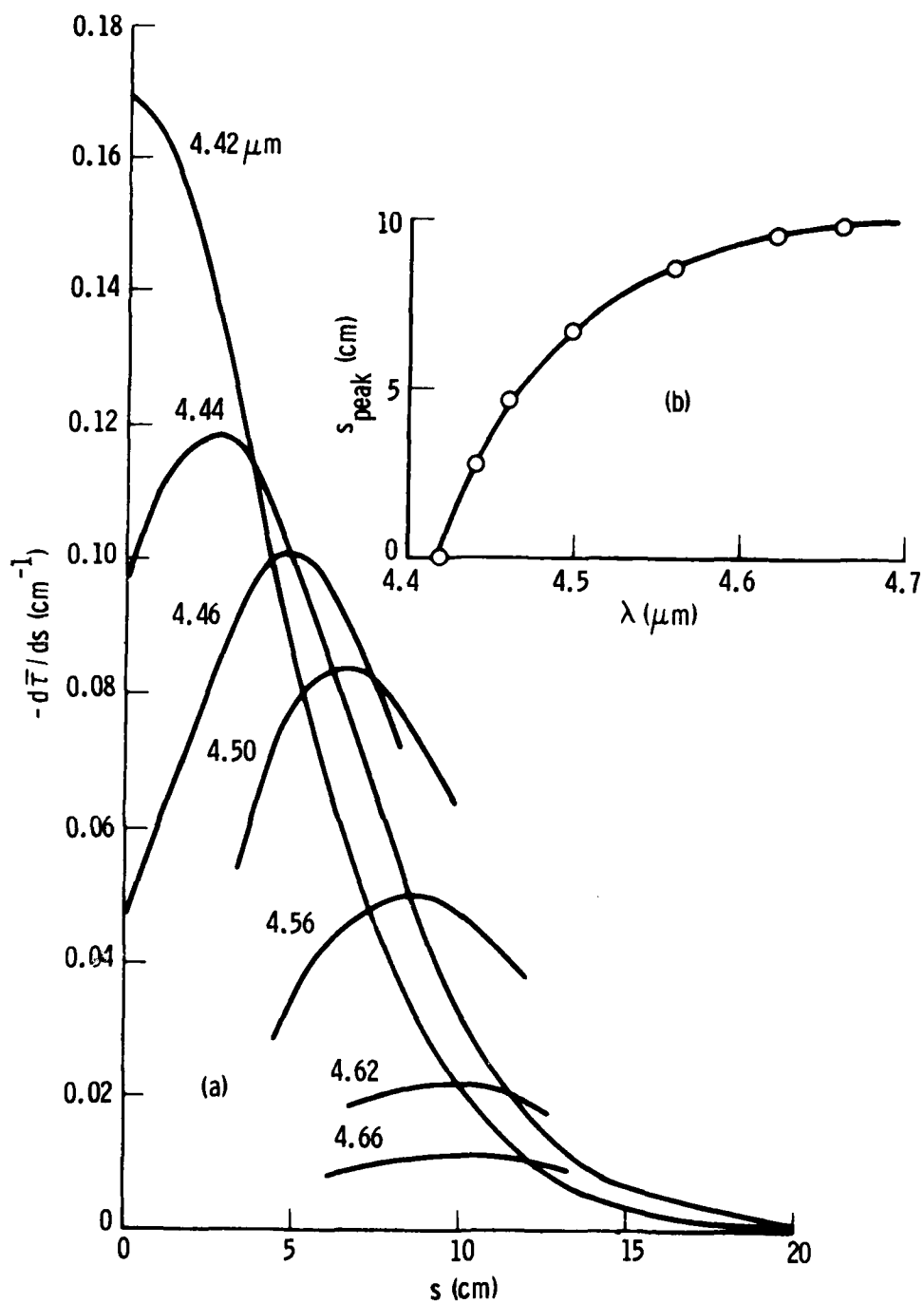


Fig. 10. Weighting functions and peak distributions for BATES model plume in CO₂ 4.3-μm red wing. (a) Weighting functions; (b) peak distribution.

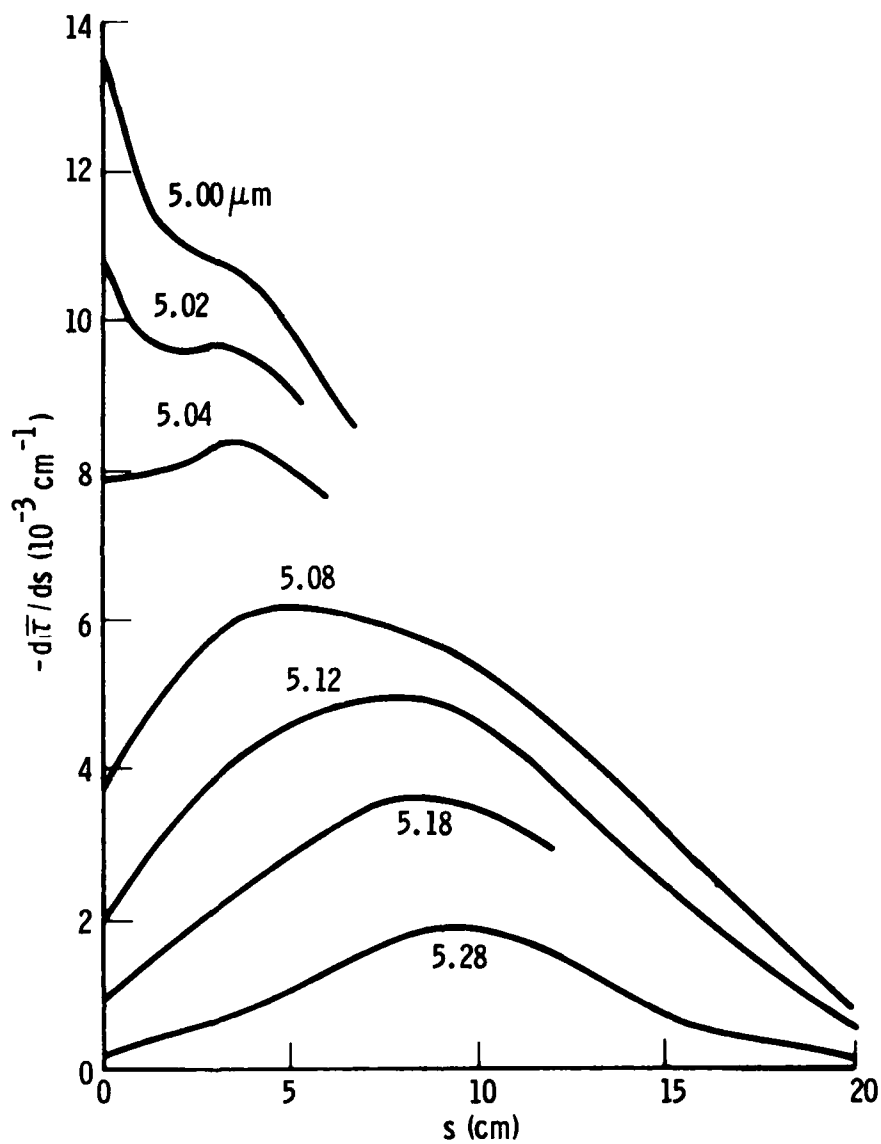


Fig. 11. Weighting functions and peak distributions for BATES model plume in CO 4.6- μm red wing. (a) Weighting functions; (b) peak distribution.

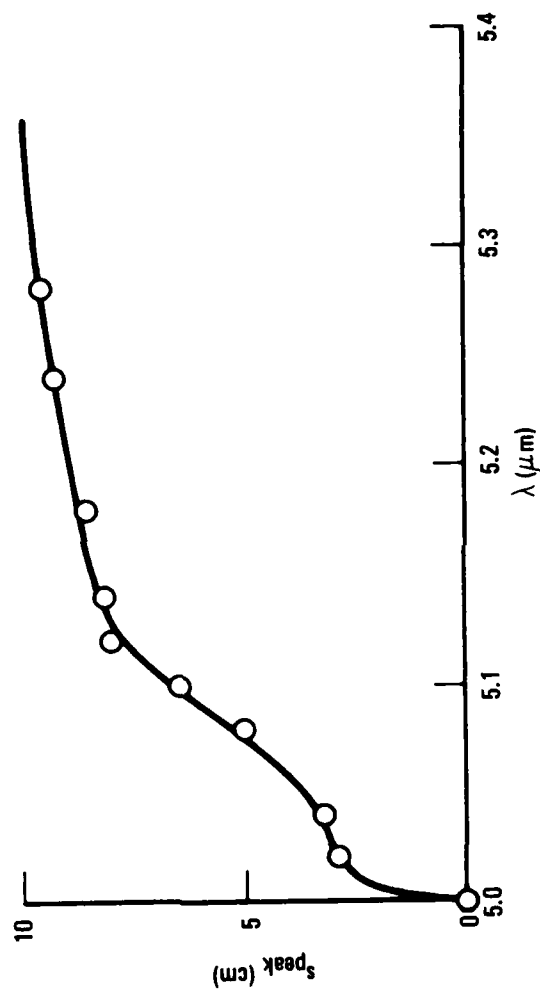


Fig. 11 (Continued). Weighting functions and peak distributions for
 BATES model plume in CO 4.6- μm red wing.
 (a) Weighting functions; (b) peak distribution

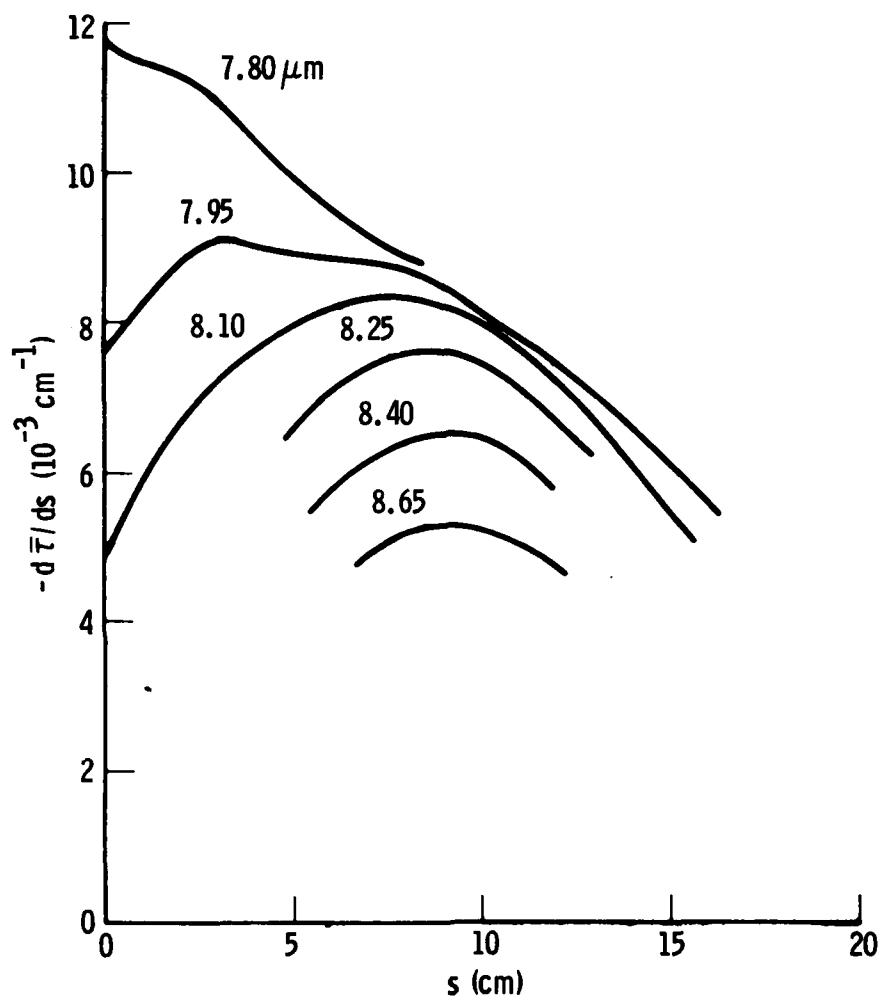


Fig. 12. Weighting functions and peak distributions for BATES model plume in H_2O 6.3- μm red wing. (a) Weighting functions; (b) peak distribution.

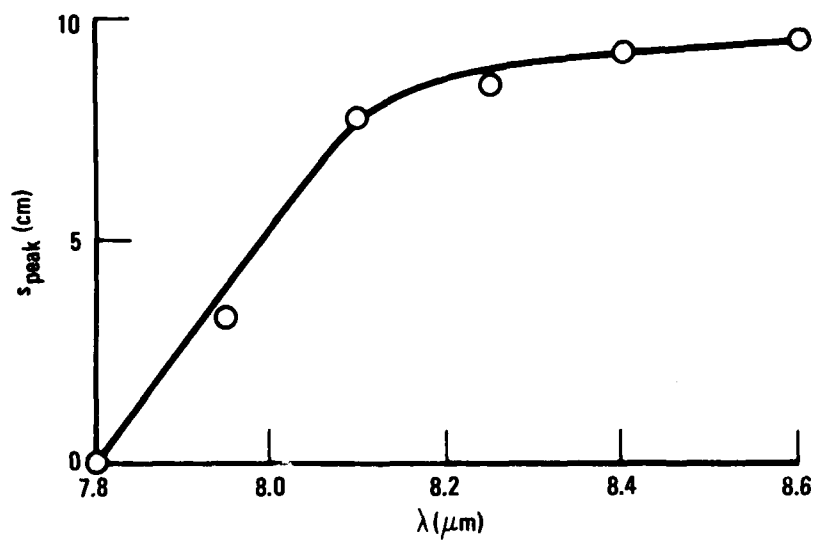


Fig. 12. (Continued) Weighting functions and peak distributions for BATES model plume in H_2O 6.3- μm red wing. (a) Weighting functions; (b) peak distribution.

inversion analysis. From part b of Figs. 10-12, a set of λ 's was selected that gave peak values at five roughly equally spaced positions across a radius of the model plume. These λ , the corresponding position, and the emission/absorption data at these λ are tabulated in Table 2. Multi-spectral inversions were carried out to obtain the temperature results shown in Fig. 13 and the concentration results shown in Fig. 14. For both the allowed CO and H₂O spectral regions, the spatial resolution of the method is so poor that a constant temperature across the plume is predicted. Even in the CO₂ region (which is not allowed by species overlap considerations), the resolution is not adequate to retrieve the true temperature profile, although a much better resolution is obtained than in the other two cases. The increasing ability to retrieve the temperature profile is directly related to the increased narrowing of the weighting function (Figs. 10-12) in the order H₂O (narrowest), CO, CO₂. The ability to retrieve the concentration profile (Fig. 14), on the other hand, displays the opposite trend. The percentage errors of concentration retrieval are approximately 7, 11, and 27% for H₂O, CO and CO₂, respectively.

The pTc profiles of Fig. 9 represent typical conditions for plumes of primary interest to the program for which this analysis was initiated (i. e., the BATES program). The significant conclusion reached so far is that infrared, band model multicolor inversion is not a viable diagnostic because the profiles cannot be retrieved with the desired accuracy. In order to determine if the method might be applicable to other tactical motors with slightly different

Table 2. Emission/Absorption Inversion Data for
BATES Model Plume

$\lambda(\mu\text{m})$	$s_p(\text{cm})$	$\overline{N}(\text{W}/\text{cm}^2\text{sr}-\mu\text{m})$	$\overline{\tau}$
CO ₂ 4.3- μm Red Wing			
4.42	0	0.411	0.0085
4.44	2.8	0.475	0.0207
4.47	5.2	0.540	0.0691
4.52	7.5	0.477	0.264
4.62	9.6	0.144	0.781
CO 4.6- μm Red Wing			
5.00	0	0.0570	0.857
5.04	3.0	0.0467	0.885
5.08	5.0	0.0367	0.913
5.12	7.7	0.0287	0.933
5.26	9.4	0.0103	0.976
H ₂ O 6.3- μm Red Wing			
7.8	0	0.0190	0.835
7.9	2.7	0.0173	0.847
8.0	5.2	0.0157	0.861
8.1	7.8	0.0142	0.871
8.6	9.5	0.0061	0.938

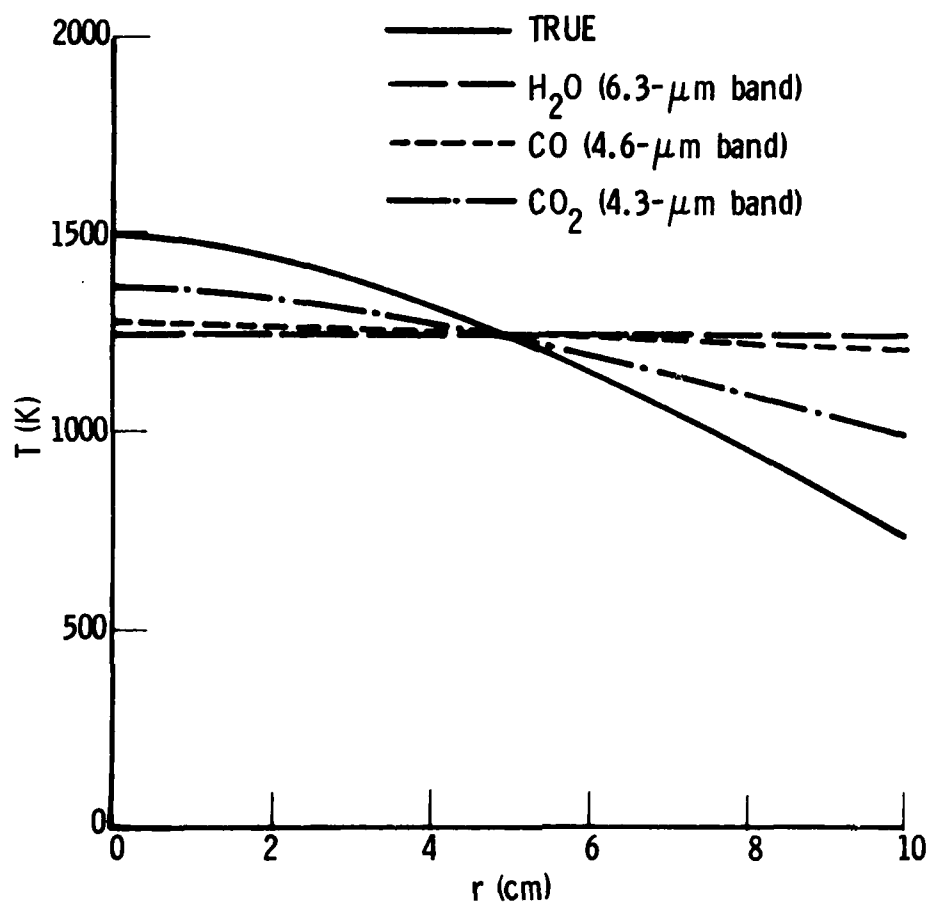


Fig. 13. Temperature inversion results for BATES model plume.

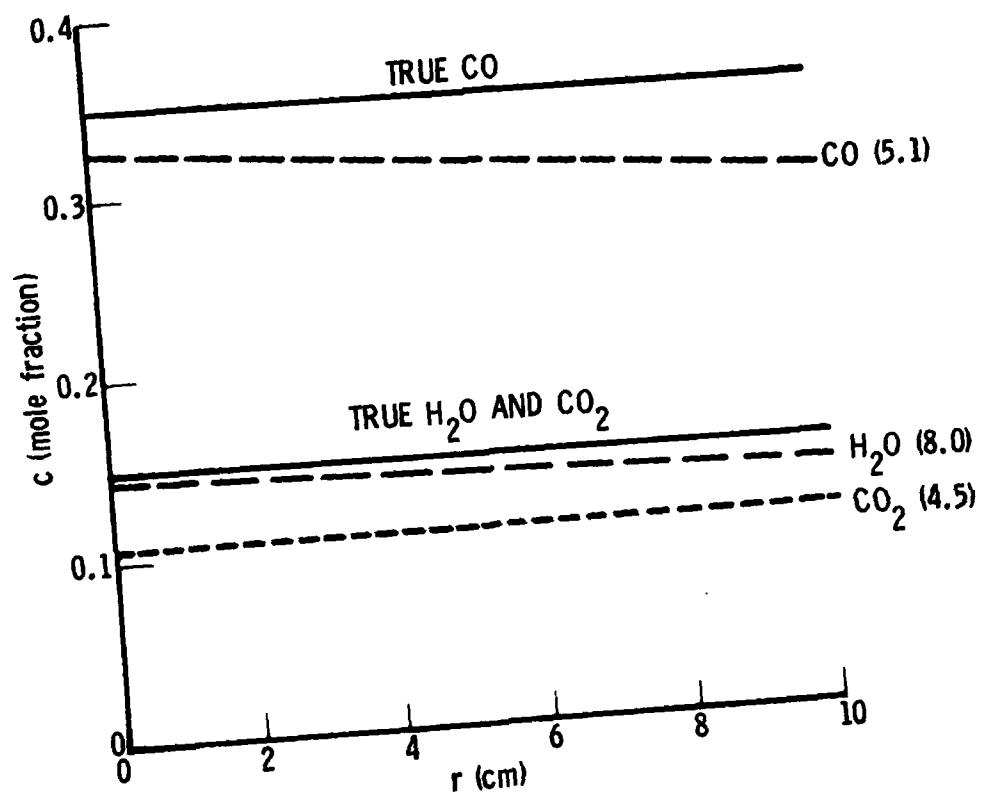


Fig. 14. Concentration inversion results for BATES model plume.

pTc profiles, two variation analyses were carried out. In the first, the temperature gradient across the plume was made stronger; in the second, the physical size of the plume was made larger.

3.3.1 Temperature Variation Analysis

In all of the spectral regions for which the weighting function peaks, the absorption band model parameter increases with temperature (at least up to ~ 2000 K). Since this increase in \bar{k} is responsible for the rising portion of the weighting function, a larger temperature gradient should result in a faster rising weighting function and thus a narrower weighting function. Here, the accuracy of retrieval for BATES-size motors (i. e., radius and concentration held constant) as a function of temperature gradient is examined. The analysis is carried out for the best possible case of inversion by considering the CO_2 4.3- μm red wing, even though this region is, in general, not available for BATES-motor analysis because of CO overlap.

The temperature profile is assumed to be a parabola symmetric about the plume center line with a value T_0 at the center line and value T_B at the plume boundary. That is,

$$T(r) = T_0 - (T_0 - T_B) \left(\frac{r}{R} \right)^2 \quad (25)$$

where R is the plume radius with value $R = 10$ cm. Emission/absorption and weighting function calculations were made for $T_0 = 500, 1000, 1500, 2000, 2500,$ and 3000 K, $T_B = 500, 1000, \dots, T_0$ and $\lambda = 4.40$ (0.02)

4.78- μm . CO_2 concentration was taken as $c = 0.15$ and pressure as $p = 1 \text{ atm}$.

Weighting function results for the sequence $T_0 = 2500 \text{ K}$ and $T_B = 2000, 1500, 1000, 500 \text{ K}$ are shown in Figs. 15-18. It can be seen that as the temperature difference between center line and boundary increases, the weighting functions become sharper, and hence we can expect a more accurate retrieval. Figure 19 displays this same narrowing of weighting function with increased temperature gradient for the sequence where the boundary temperature is maintained at 500 K while the center line temperature is increased from 1500 to 3000 K . Here, only the weighting function that peaks near $s = 3 \text{ cm}$ ($s/R \approx 0.3$) is shown. A summary of the information of this figure is made in Table 3. In particular, the decrease in peak halfwidth with increasing temperature gradient is illustrated. The limit of halfwidth for large gradients appears to be $\Delta s \approx 1/2R \approx 0.48$. This number should be compared with that obtained by Cutting and Stewart in their furnace work (0.28).

Multispectral inversions with program MUSIC were carried out for the cases of $T_0 = 1500, 2000, 2500$ and 3000 K for constant $T_B = 500 \text{ K}$. The variation in peak position of the weighting functions with wavelength for the four cases is shown in Fig. 20. From these plots, a set of λ 's was determined to give coverage of the plume at distances of 1, 3, 5, 7 and 9 cm into the plume. These values of λ and the emission/absorption data at these λ are tabulated in Table 4. The selection of λ 's was somewhat modified

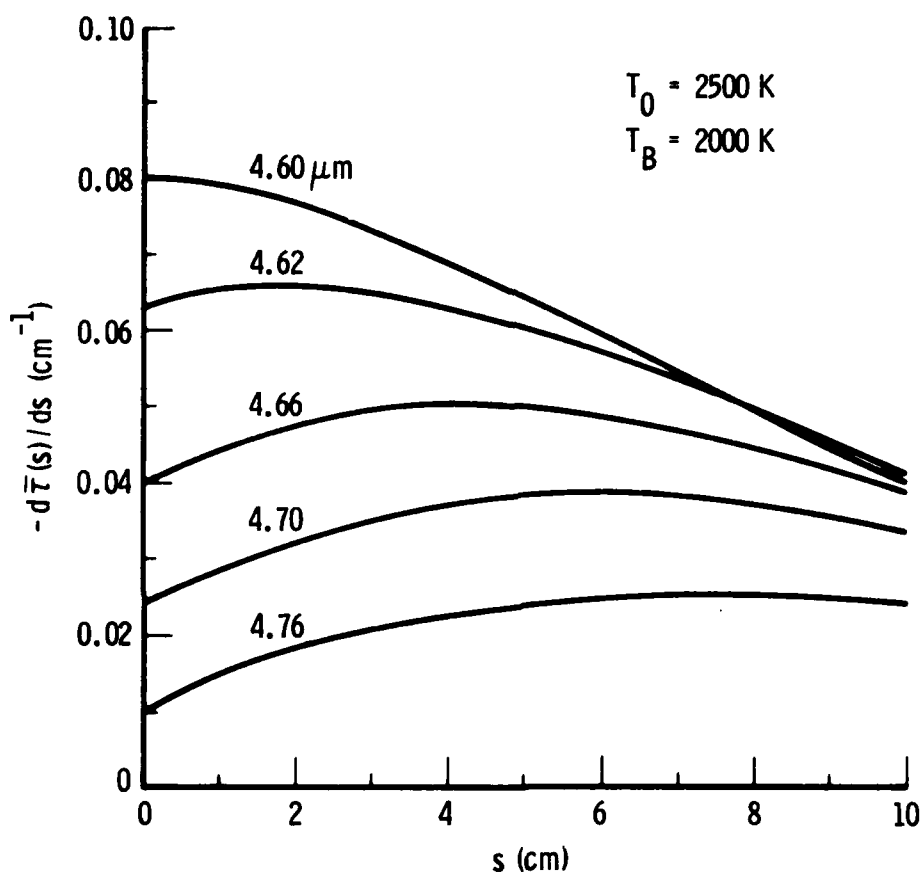


Fig. 15. Weighting functions for $T_0 = 2500 \text{ K}$ and $T_B = 2000 \text{ K}$.

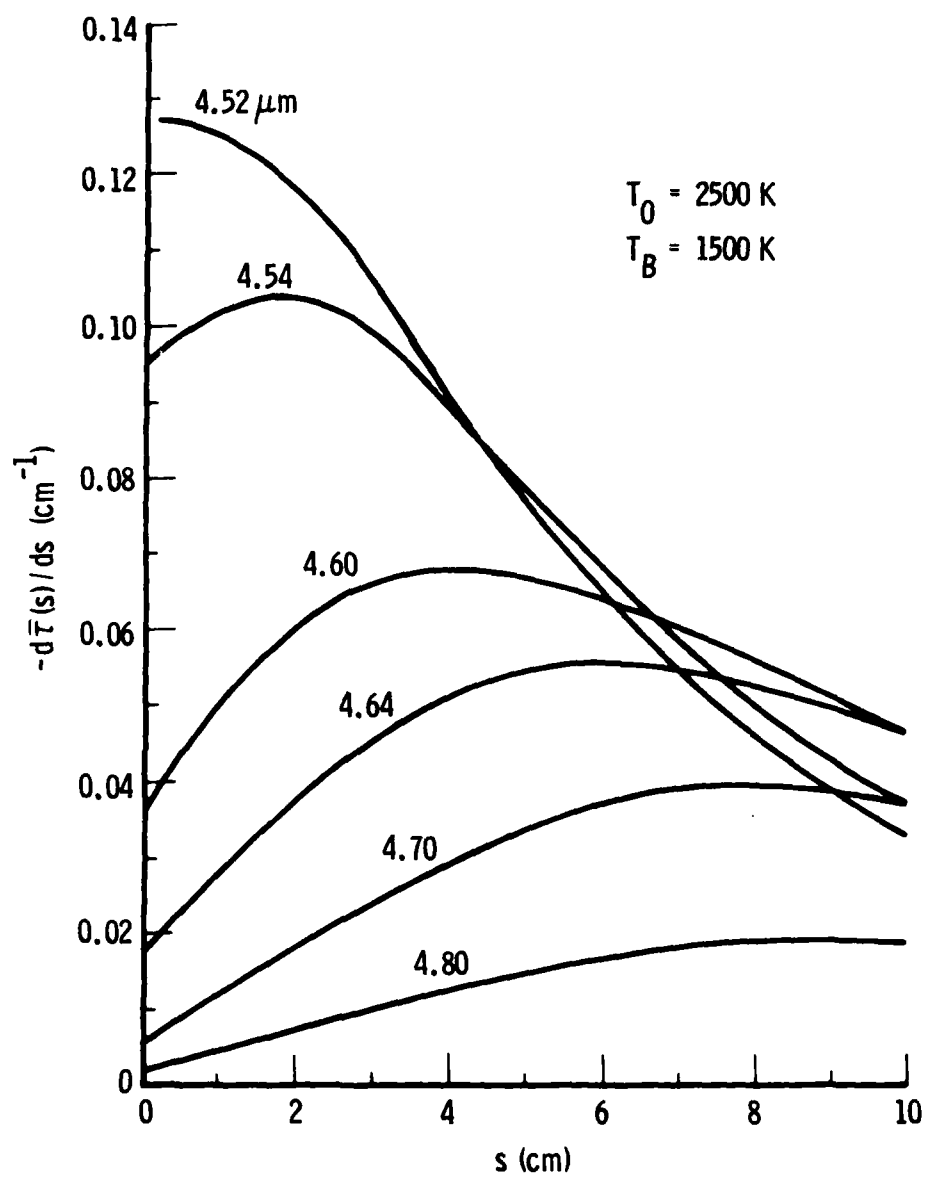


Fig. 16. Weighting functions for $T_0 = 2500 \text{ K}$ and $T_B = 1500 \text{ K}$.

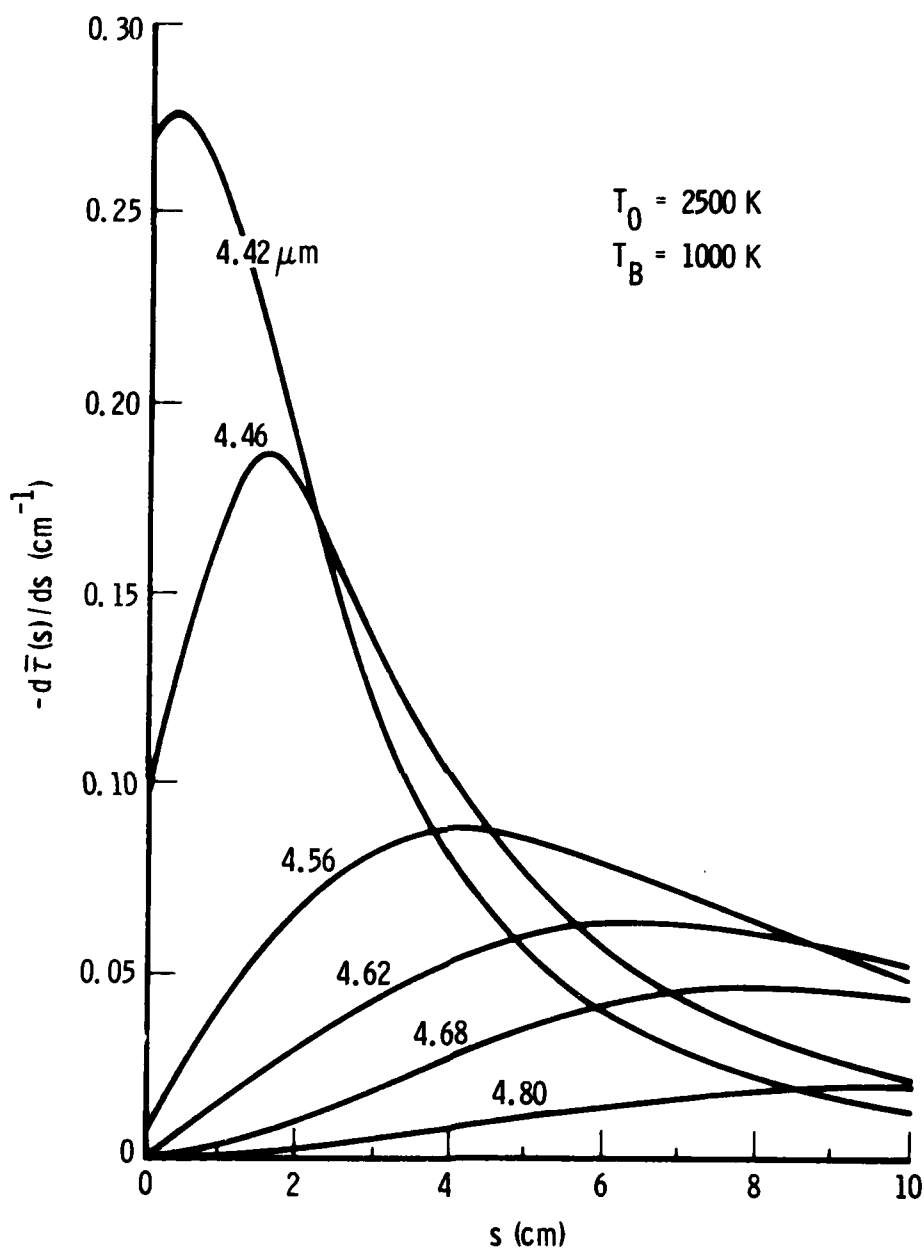


Fig. 17. Weighting functions for $T_0 = 2500 \text{ K}$ and $T_B = 1000 \text{ K}$.

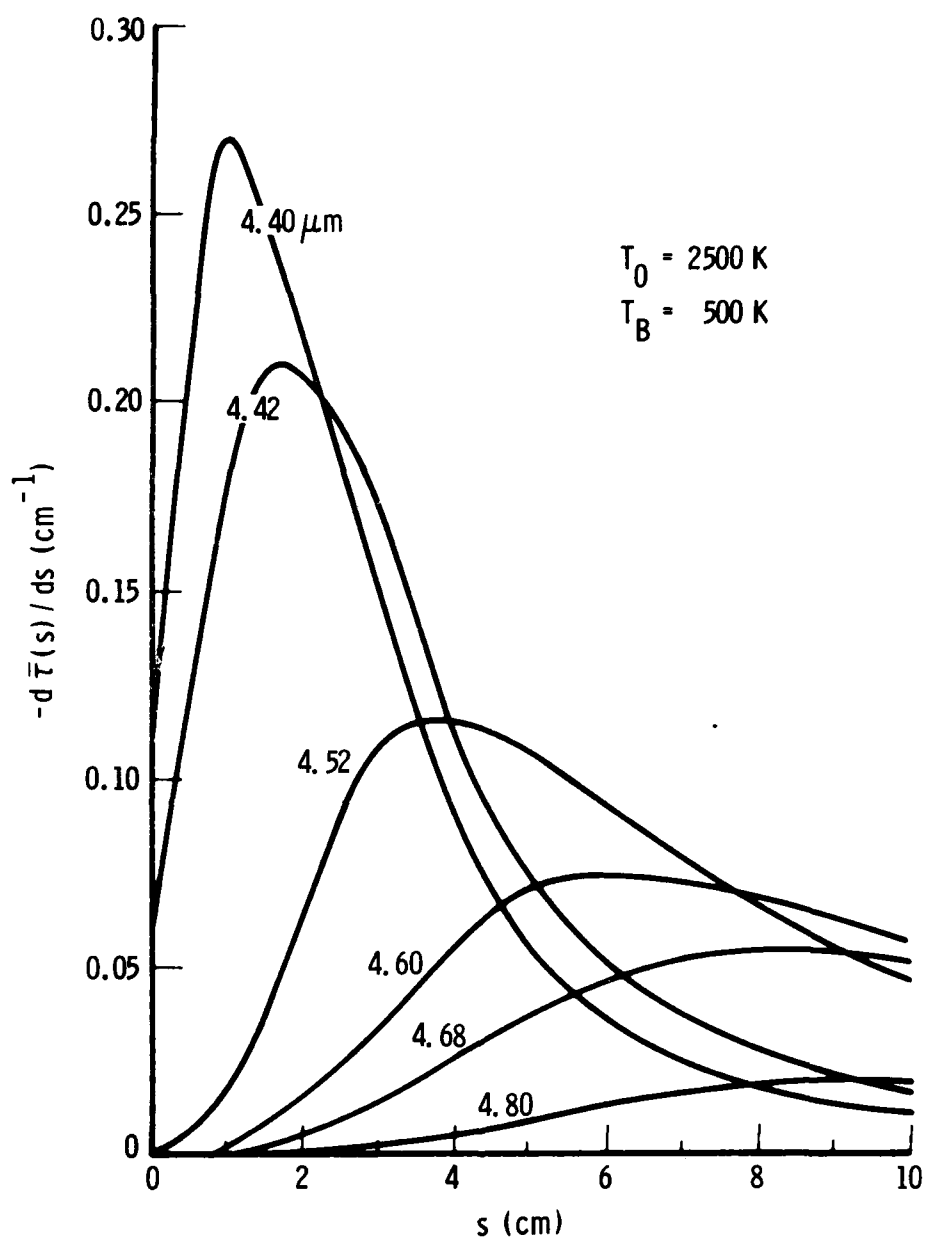


Fig. 18. Weighting functions for $T_0 = 2500 \text{ K}$ and $T_B = 500 \text{ K}$.

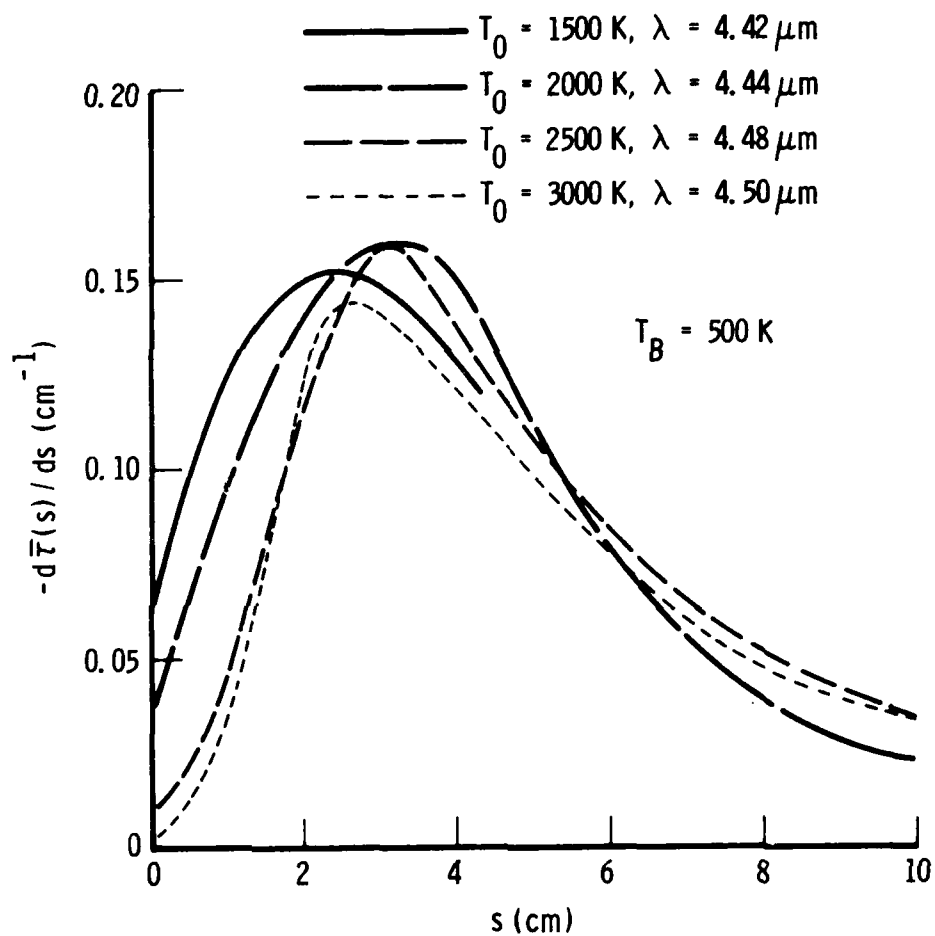


Fig. 19. Variation in weighting function with temperature gradient. For different temperature conditions, the weighting functions are those that peak near $s/R = 0.3$.

Table 3. Variation of Weighting Function Half-Width (FWHM)
with Temperature Gradient

$T_0(K)$	$\lambda(\mu m)$	$s_p(cm)$	$\Delta s_{\frac{1}{2}}(cm)$
1500	4.42	2.4	6.0
2000	4.44	3.2	5.3
2500	4.48	3.1	4.8
3000	4.50	2.6	4.8

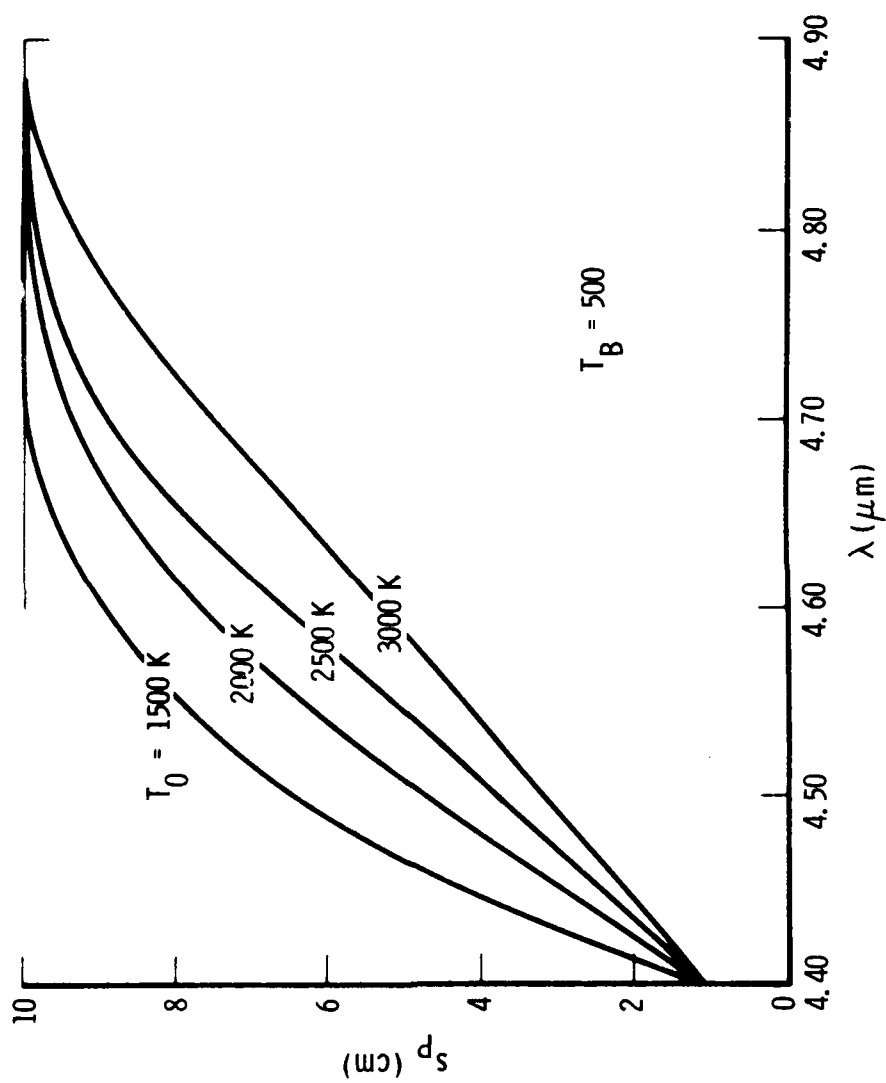


Fig. 20. Variation in peak distribution with temperature gradient.

Table 4. Emission/Absorption Inversion Data for Temperature Gradient Variation

$\lambda(\mu\text{m})$	$s_p(\text{cm})$	$\bar{N}(\text{w}/\text{cm}^2\text{-sr-}\mu\text{m})$	$\bar{\tau}$
$T_0 = 1500 \text{ K}$			
4.40	1	0.333	0.0037
4.42	3	0.425	0.010
4.46	5	0.556	0.055
4.52	7	0.493	0.270
4.60	9	0.202	0.708
$T_0 = 2000 \text{ K}$			
4.40	1	0.578	0.0031
4.44	3	0.841	0.012
4.52	5	1.030	0.119
4.58	7	0.815	0.341
4.68	9	0.316	0.743
$T_0 = 2500 \text{ K}$			
4.40	1	0.866	0.0050
4.48	3	1.431	0.033
4.52	5	1.527	0.112
4.62	7	1.221	0.333
4.70	9	0.733	0.599
$T_0 = 3000 \text{ K}$			
4.40	1	1.173	0.009
4.50	3	1.933	0.054
4.60	5	1.890	0.204
4.68	7	1.449	0.402
4.78	9	0.823	0.653

so that all transmittance were greater than ~ 0.003 . This was judged to be a lower bound on measurable transmittance.

A typical example of the iteration inversion behavior is shown in Fig. 21 for the case $T_0 = 2000$ K and $T_B = 500$ K. ΔT_{rms} and Δc_{rms} are the root-mean-square differences between successively iterated profiles for temperature and concentration, respectively. Final convergence for this case is taken at $i = 11$ where the ΔT curve bottoms out. Comparisons between the true parabolic temperature profiles and the final retrieved profiles are shown in Fig. 22. In all cases, the retrieved profile is flatter than the true profile and underpredicts the true value at the center line and overpredicts at the boundary. The accuracy of center line prediction increases with increasing gradient while the accuracy of boundary prediction worsens. Quantitative assessment of overall profile prediction accuracy is shown in Fig. 23. In the left-hand figure, the difference between the retrieved center line and boundary temperature is plotted against the true temperature difference. In the right-hand figure, the ratio of retrieved temperature difference to true temperature difference is plotted against the true difference. This second figure indicates that the "overall accuracy" of the inversion increases with increasing gradient and approaches a constant underprediction of $\sim 30\%$ for strong gradients. If one is not so concerned about the accuracy of the whole profile, the accuracy of inversion is better. For example, if only the center region of the plume between $0 \leq r \leq 7$ cm is of concern, Fig. 22 indicates that temperature accuracies of between 5 and 10% can be obtained.

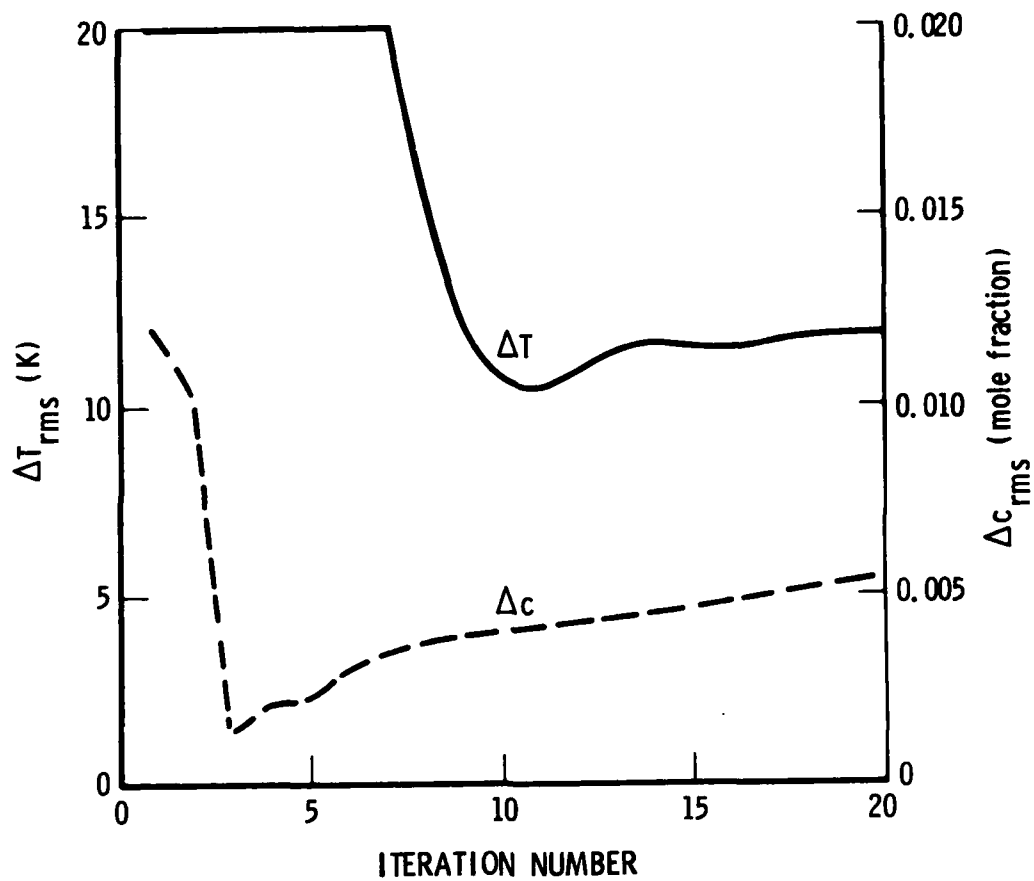


Fig. 21. Convergence behavior for temperature and concentration residuals.
 $T_0 = 2000 \text{ K}$, $T_B = 500 \text{ K}$.

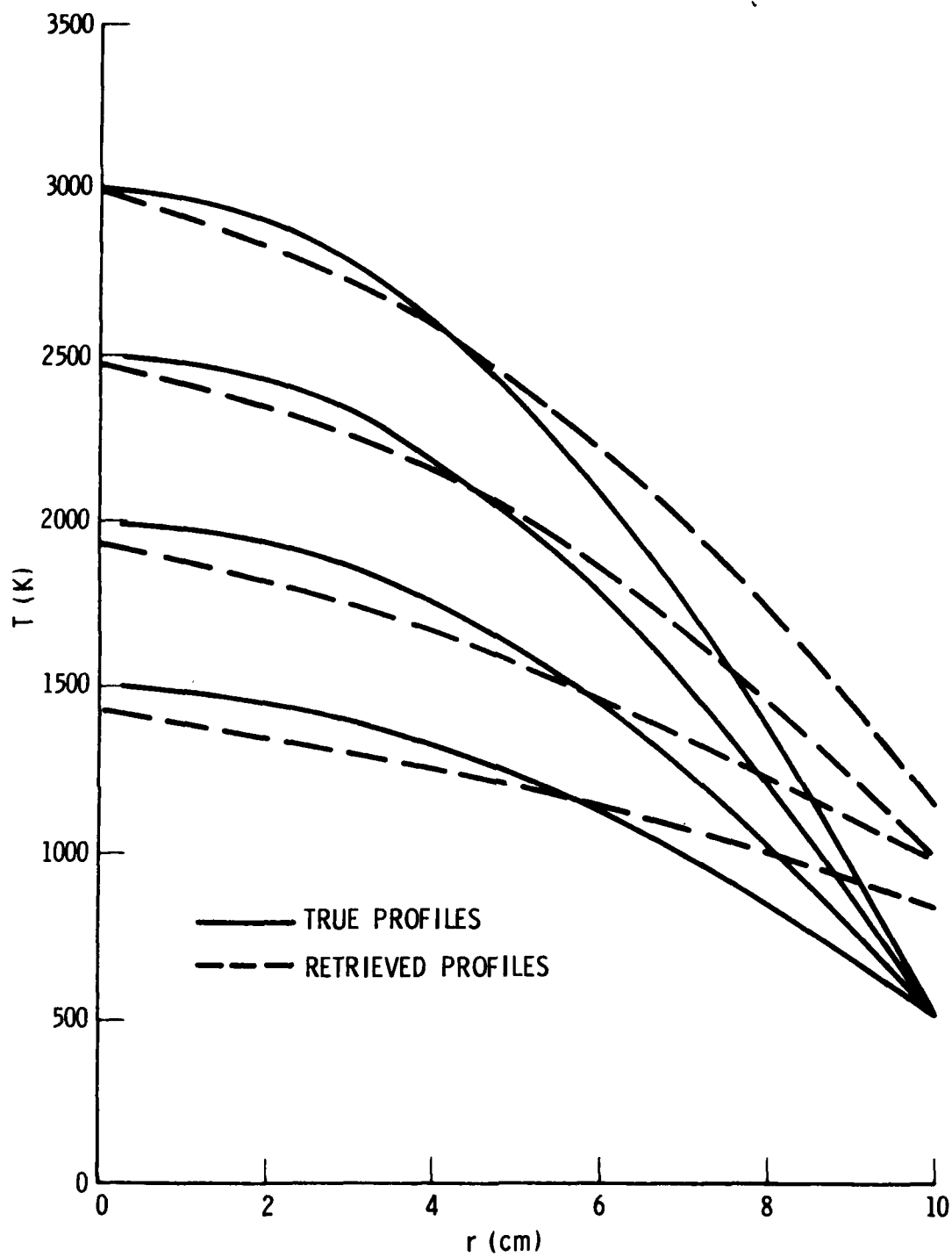


Fig. 22. Temperature inversion results for four temperature gradient cases.

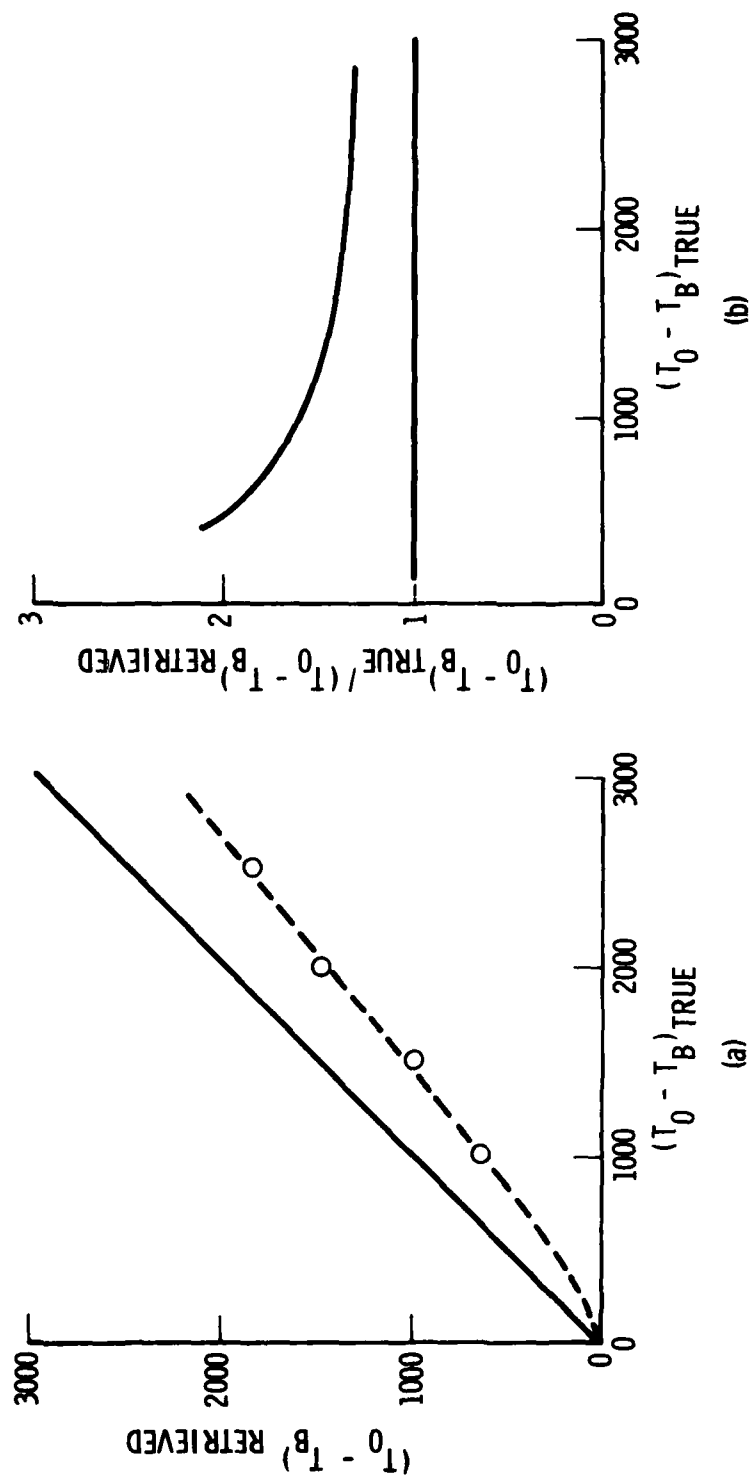


Fig. 23. Variation of temperature inversion accuracy with temperature gradient.
(a) absolute error; (b) relative error.

Comparisons between retrieved and true concentration profiles are shown in Fig. 24. In all cases, the accuracy of retrieval is poor and worsens with increasing temperature gradient. This is true even if we restrict ourselves to the central portion of the plume.

In summary, the main conclusions are that (1) the accuracy of temperature retrieval increases as the temperature gradient increases, (2) the accuracy of concentration retrieval worsens as the temperature gradient increases, and (3) that under no conditions studied could the accuracy of retrieval be considered as good. The impact of this last conclusion is compounded by the fact that the analysis was carried out in the 4.3- μ m red wing which is the best possible spectral region for inversion. Worse results would obtain in other spectral regions.

3.3.2 Size Variation Analysis

The success of multispectral inversions rests on the narrowness of the weighting function $-d\tau(\lambda, s)/ds$. For nominal BATES-motor plume conditions (e.g., size, temperature profile, concentration), the weighting functions are not narrow enough to yield a good retrieval. It has just been shown that plumes with the same optical thickness as the BATES motors but with larger temperature gradients lead to somewhat narrower weighting functions (and thus more accurate retrieval) but still not narrow enough to yield what could be called a good inversion. Here, the effect of increased optical thickness on accuracy of retrieval is examined for a fixed temperature profile. The optical thickness is varied by retaining a fixed concentration

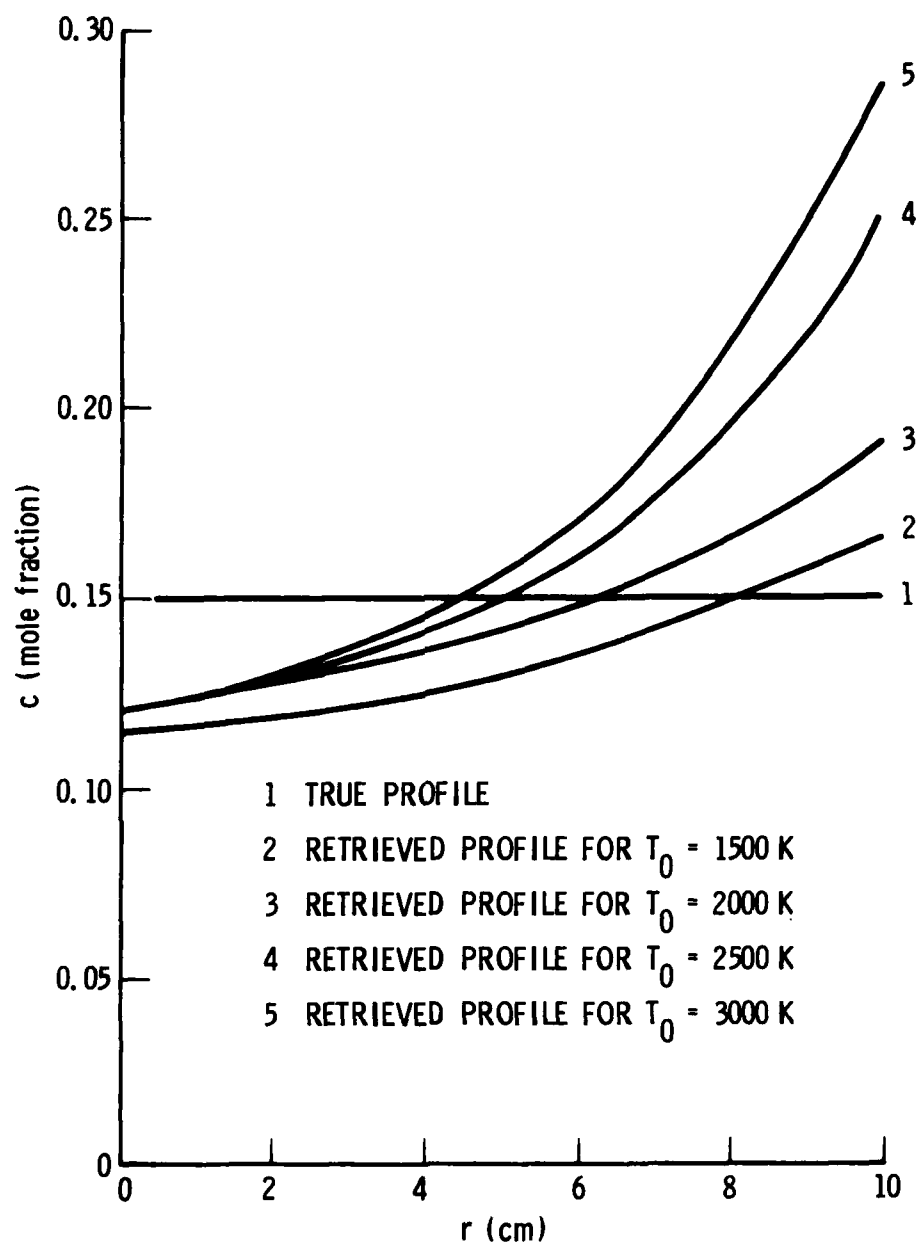


Fig. 24. Concentration inversion results for four temperature gradient cases.

while increasing the physical size of the plume. The analysis is again carried out in the red wing of the $4.3\text{-}\mu\text{m CO}_2$ band.

The temperature profile is parabolic with $T_0 = 1500\text{ K}$ and $T_B' = 500\text{ K}$. The concentration is $c = 0.15$, the total pressure is $p = 1\text{ atm}$ and plume radii of $R = 10, 20, 30, 40$ and 50 cm are employed. An example of the sharpening of the weighting functions with increasing radius is shown in Fig. 25. The weighting functions are those that peak near $s/R = 0.3$ and have been normalized to unity at their peaks. With increasing radius, the sharpening results from a faster fall-off of the trailing edge of the function. This should be compared to the case of increasing temperature gradient (Fig. 19) where the sharpening was due primarily to a faster rise of the leading edge.

The halfwidths (divided by R) of the weighting functions that peak around $s/R = 0.3$ are plotted in Fig. 26 versus plume radius and tabulated in Table 5. A continual decrease in halfwidth with increasing R is evident, and the trend is not incompatible with the value obtained by Cutting and Stewart in their furnace work.

Multispectral inversions with program MUSIC were carried out for the five radius cases. The variations in peak position of the weighting functions with wavelength are shown in Fig. 27. From these plots, a set of λ 's was determined to give coverage of the plume at distances of $s/R = 0.1, 0.3, 0.5, 0.7$ and 0.9 into the plume. These sets of λ and the E/A data at these λ are tabulated in Table 6. A feature that has not appeared in

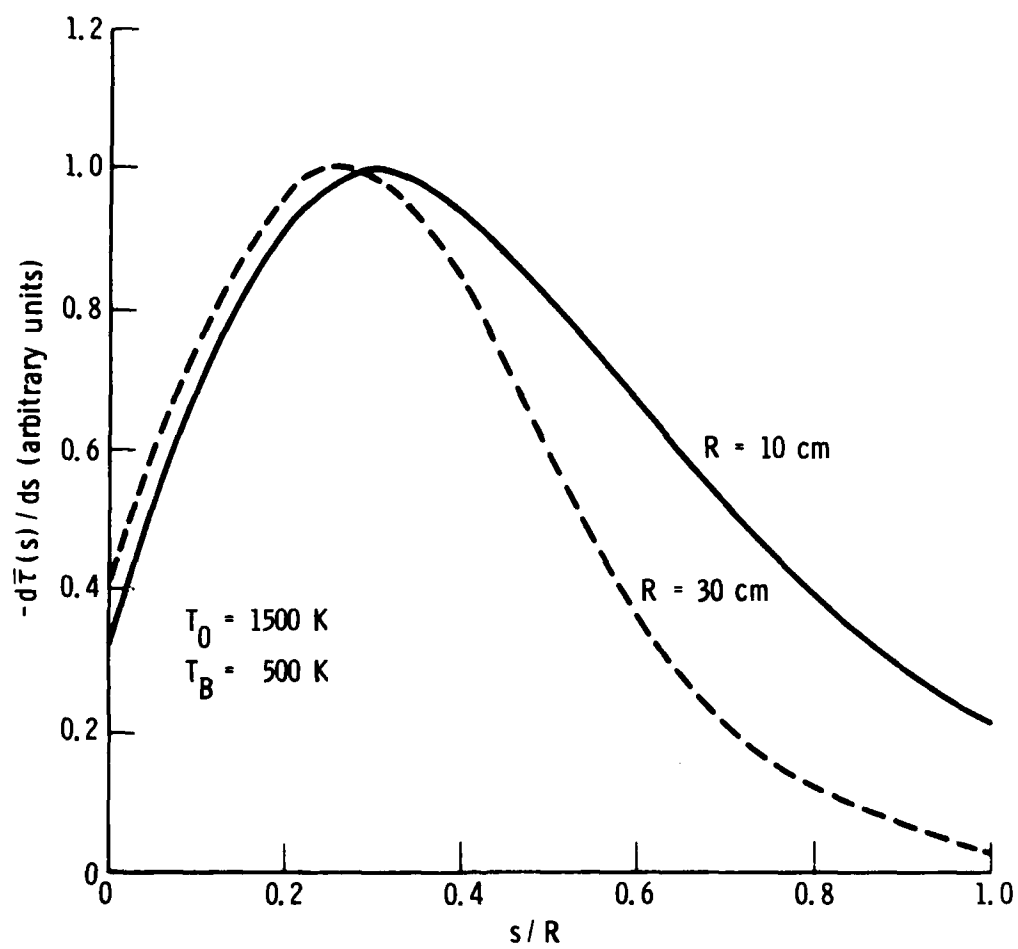


Fig. 25. Variation in weighting function with plume radius.

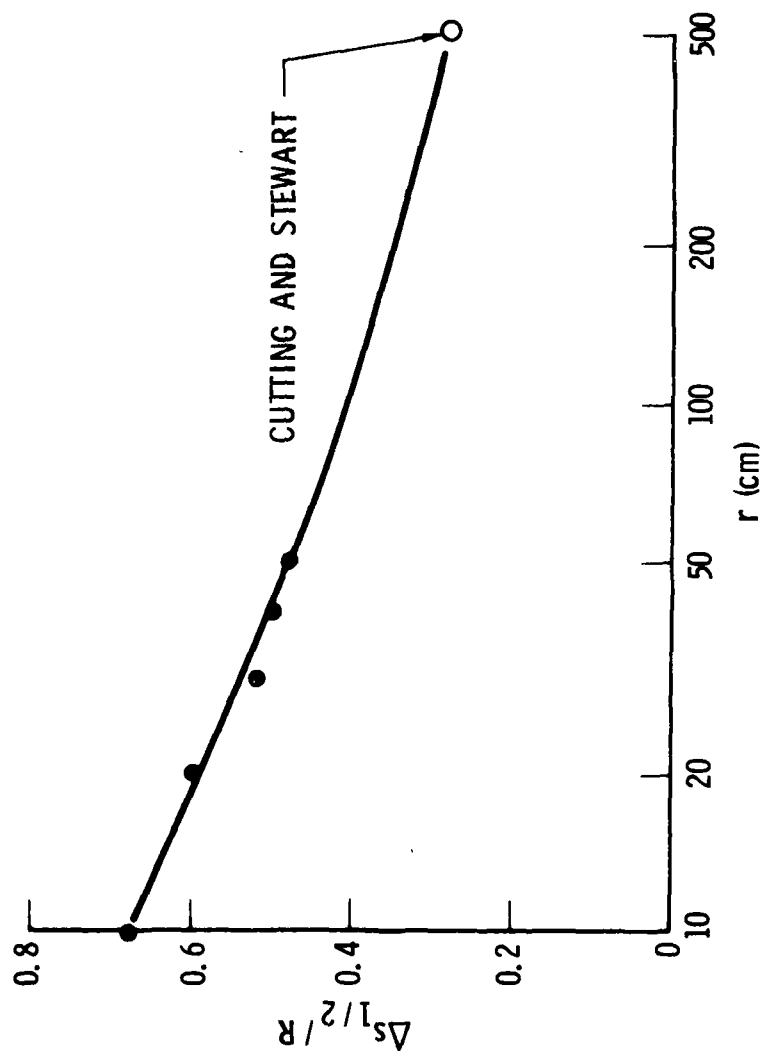


Fig. 26. Variation in weighting function half-width (FWHM) with plume radius.

Table 5. Variation of Weighting Function Half-Width (FWHM)
with Plume Radius

R (cm)	λ (μm)	s_p/R	$\Delta s_p/R$
10	4.43	.30	.68
20	4.45	.34	.60
30	4.45	.25	.52
40	4.46	.25 and .33	.50
50	4.47	.28	.48

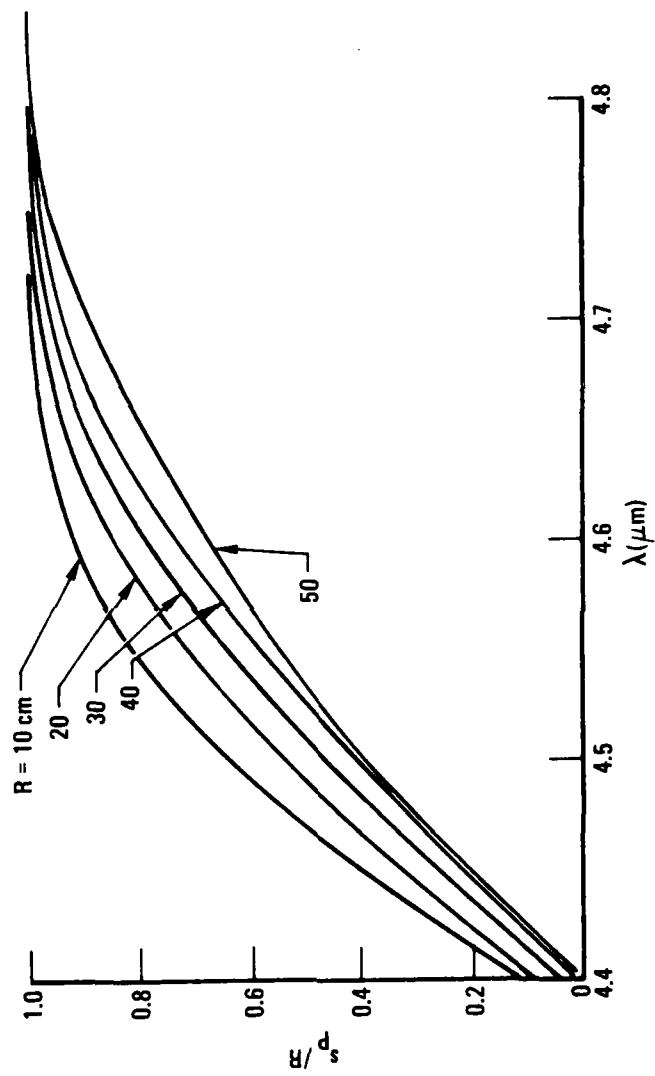


Fig. 27. Variation in peak distribution with plume radius.

Table 6. Emission/Absorption Inversion Data for
Plume Radius Variation

λ (μm)	s_p/R	\bar{N} ($\text{W}/\text{cm}^2\text{-sr-}\mu\text{m}$)	$\bar{\tau}$
R = 10 cm			
4.40	1	.3309	.0036
4.43	3	.4639	.016
4.47	5	.5631	.074
4.51	7	.5218	.218
4.59	9	.2319	.664
R = 20 cm			
4.40	1	.2011	0
4.45	3	.4266	.0027
4.49	5	.5687	.023
4.55	7	.5382	.204
4.63	9	.2248	.668
R = 30 cm			
4.41	1	.1764	0
4.45	3	.3458	.0003
4.51	5	.5730	.015
4.57	7	.5507	.183
4.65	9	.2309	.653
R = 40 cm			
4.42	1	.1726	0
4.46	3	.3445	.0001
4.52	5	.5651	.0086
4.59	7	.5395	.203
4.67	9	.2137	.674
R = 50 cm			
4.43	1	.1767	0
4.47	3	.3406	0
4.53	5	.5634	.0064
4.61	7	.5099	.244
4.69	9	.1859	.709

previous work is evident in this tabulation. For R greater than the nominal BATES motor radius of ~ 10 cm, the transmittance through the plume is immeasurably small at those wavelengths that give weighting functions that peak in the outer zones of the plume. Thus, for plumes with optical thickness $u = cp2R$ greater than about (0.15) (1 atm) (2) (10 cm) = 30 atm-cm, no inversion can be made for concentration. Only the temperature profile (in principle) can be retrieved. (The furnace work of Cutting and Stewart was concerned only with temperature retrieval.) Accordingly, MUSIC was modified to perform inversion with the concentration set to the known values $c = 0.15$. The results of the temperature inversion are shown in Fig. 28. As would be expected from the narrowing of the weighting functions with increasing R , the accuracy of retrieval increases with R . Again, however, the accuracy of retrieval cannot be called good. The mean error over the profile is $\sim 15\%$ for $R > 30$ cm, and greater for smaller R . Apparently, only for optical depths very much greater than those obtained in tactical missiles do the widths of the weighting functions get small enough to allow accurate inversion.

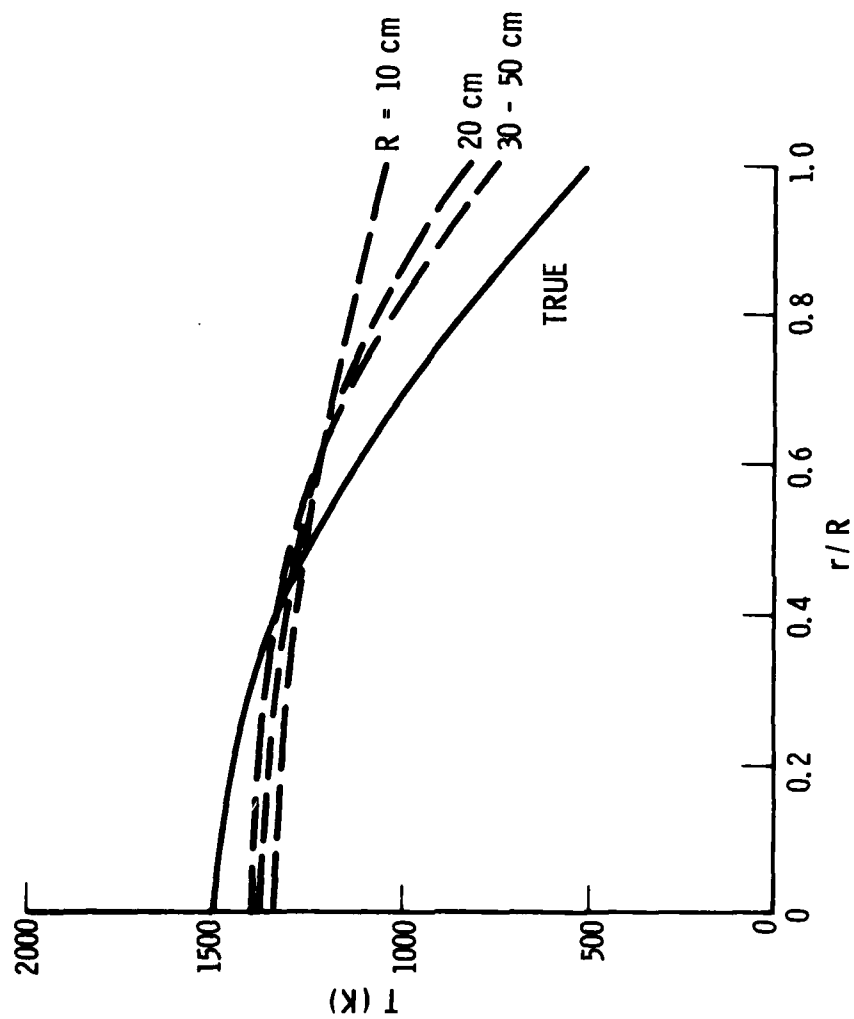


Fig. 28. Temperature inversion results for four plume radii.

4. MONOCHROMATIC APPLICATION

The principal result obtained so far is that the optical path weighting function $-d\bar{\tau}(s)/ds$ is not sharp enough to allow multicolor inversion of BATES plume data on a band model spectral scale. In this Section, the feasibility of multicolor inversion on a monochromatic spectral scale is examined. No consideration is given to the experimental problem of obtaining monochromatic data, but only the usefulness of such data for inversion if it were available. The first Section (4.1) considers the analytic form of the weighting function for a triangular plume profile. Application of the result is made to molecular infrared lines and atomic visible lines in Sections 4.2 and 4.3, respectively. For the infrared application, it is found that although the monochromatic weighting functions are sharper than the band model functions, they are still not sharp enough. In addition, it is difficult to define conditions such that the peaks of the weighting functions for different λ are distributed over the whole plume (i. e., from boundary to center line). The atomic line functions are much sharper and could, in principle, provide a decent inversion. Unfortunately, other considerations obviate the method. The last Section (4.4) briefly treats the weighting functions on the integrated line spectral scale. In this entire Section, only the weighting functions are considered; no inversion analyses per se are carried out.

4.1 Monochromatic Weighting Functions

The spectral transmittance between $s = 0$ and general path position

s is

$$\tau(\lambda, s) = \exp \left[- \int_0^s c(s') p(s') k(\lambda, s') ds' \right] \quad (26)$$

where c is mole fraction of active gas, p is total gas pressure, and k is the absorption coefficient. The weighting function is

$$\frac{-d\tau(\lambda, s)}{ds} = c(s) p(s) k(\lambda, s) \tau(\lambda, s). \quad (27)$$

For an isolated Lorentz line, the absorption coefficient is

$$k(\lambda, s) = \frac{S(s)}{\pi} \frac{\gamma(s)}{\nu^2 + \gamma^2(s)} \quad (28)$$

where S(s) is the line strength, $\gamma(s)$ is the line width, and $\nu = 1/\lambda$.

In order to simplify the analysis, assume c(s), p(s) and $\gamma(s)$ are constants with s (neglect the weak $T^{-1/2}$ dependence of γ on T), and approximate the temperature variation of line strength by

$$S(T) = \frac{\sigma_0}{T} e^{-\theta/T} \quad (29)$$

where θ is the lower level energy expressed in temperature units and σ_0 is an intrinsic line strength.

Also, consider a simple linear temperature variation along the optical path given by

$$T(s) = \begin{cases} T_B + \beta s & 0 \leq s \leq R \\ (2T_0 - T_B) - \beta s & R \leq s \leq 2R \end{cases} \quad (30)$$

where $\beta = (T_0 - T_B)/R$ (Fig. 29). As an approximation to a plume, T_B is the plume boundary temperature, T_0 is the centerline temperature and R is the plume radius.

Use of these assumptions in Eqs. 26 and 27 yields

$$-\frac{d\tau(\lambda, s)}{ds} = \frac{2\chi_0\beta}{\theta} \left[\frac{\theta}{T(s)} \right] \tau(\lambda, s) e^{-\theta/T(s)} \quad (31)$$

where

$$\tau(\lambda, s) = \exp \left\{ -2\chi_0 \left[E_1 \left(\frac{\theta}{T(s)} \right) - E_1 \left(\frac{\theta}{T_B} \right) \right] \right\} \quad (32)$$

for $0 \leq s \leq R$,

$$\tau(\lambda, s) = \exp \left\{ -2\chi_0 \left[2E_1 \left(\frac{\theta}{T_0} \right) - E_1 \left(\frac{\theta}{T_B} \right) - E_1 \left(\frac{\theta}{T(s)} \right) \right] \right\} \quad (33)$$

for $R \leq s \leq 2R$,

$$\chi_0 = \frac{cp\gamma \sigma_0 / \beta}{2\pi (\nu^2 + \gamma^2)} \quad (34)$$

and $E_1(z)$ is the exponential integral of order 1. The formation of a peak in Eq. 31 is caused by the opposing actions of the increase in $e^{-\theta/T(s)}$ with s and the decrease of $\tau(\lambda, s)$ with s . In order to obtain a sharp rise in the weighting function, θ should be large (that is, we must look at a hot line) and in order to obtain a sharp fall-off, the intrinsic line strength σ_0 should be large. The position at which the weighting function peaks is determined by setting

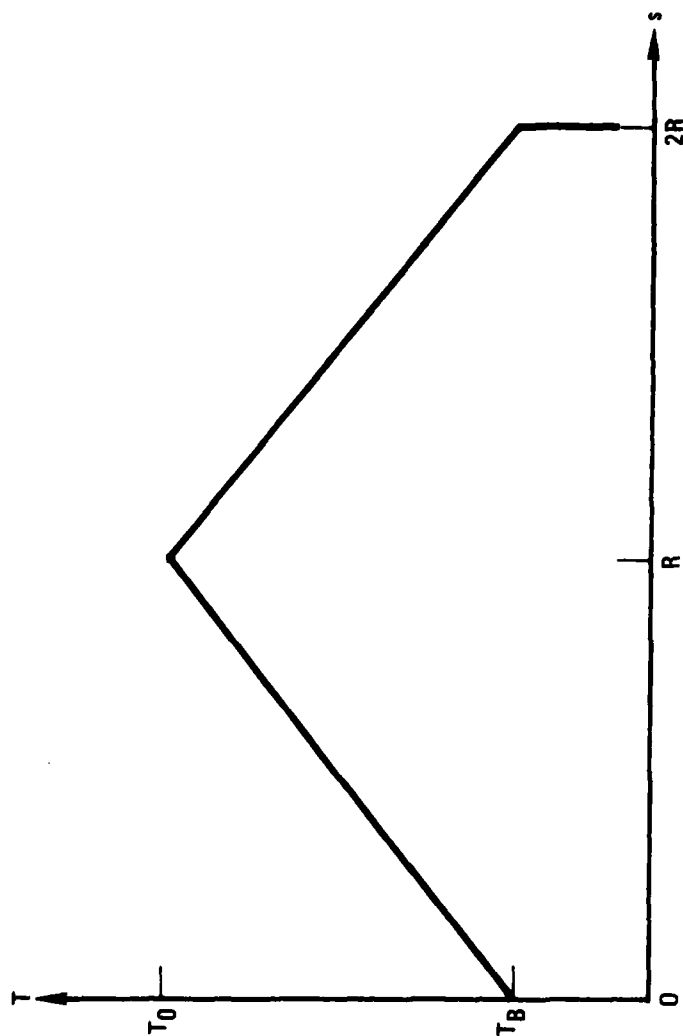


Fig. 29. Triangular temperature profile for monochromatic analysis.

$d^2\tau(\lambda, s)/ds^2 = 0$. The result is

$$\chi_o = \frac{1}{2} \left[\frac{\theta}{\tau(s)} - 1 \right] e^{\theta/\tau(s)} \quad (35)$$

If the weighting function has a peak, it always occurs for $S \leq R$ (because the temperature gradient is negative for $S > R$ and a peak cannot be formed in a region of negative gradient).

4.2 Application to Molecular Lines

Consider a molecular line with the properties

$$\sigma_o = 6 \times 10^3 \text{ cm}^{-2} \text{ K/atm,}$$

$$\theta = 3200\text{K,}$$

$$\gamma = 0.1 \text{ cm}^{-1}$$

These data are representative of the strongest CO line in the $\nu' = 2 \rightarrow \nu'' = 1$ fundamental band. As an approximation to the BATES engine, assume $c = 0.1$, $p = 1 \text{ atm}$, $T_B = 800 \text{ K}$, $T_o = 1500 \text{ K}$, and $\beta = 70 \text{ K/cm}$. The two weighting functions that result for the line center ($\nu = o$) and the half-height position ($\nu = \gamma$) are shown in Fig. 30. The curve for $\nu = \gamma$ could also be interpreted as the curve that would obtain at the center of a line with $\sigma_o = 3 \times 10^3 \text{ cm}^{-2} \text{ K/cm}$ (that is, half as strong).

Two important features of these curves are: 1) they are sharper than the corresponding curves for band model resolution, and 2) the entire spatial region between $0 \leq s \leq R$ cannot be covered. That the curves are sharper than the band model curves is illustrated in Fig. 31. The comparison is

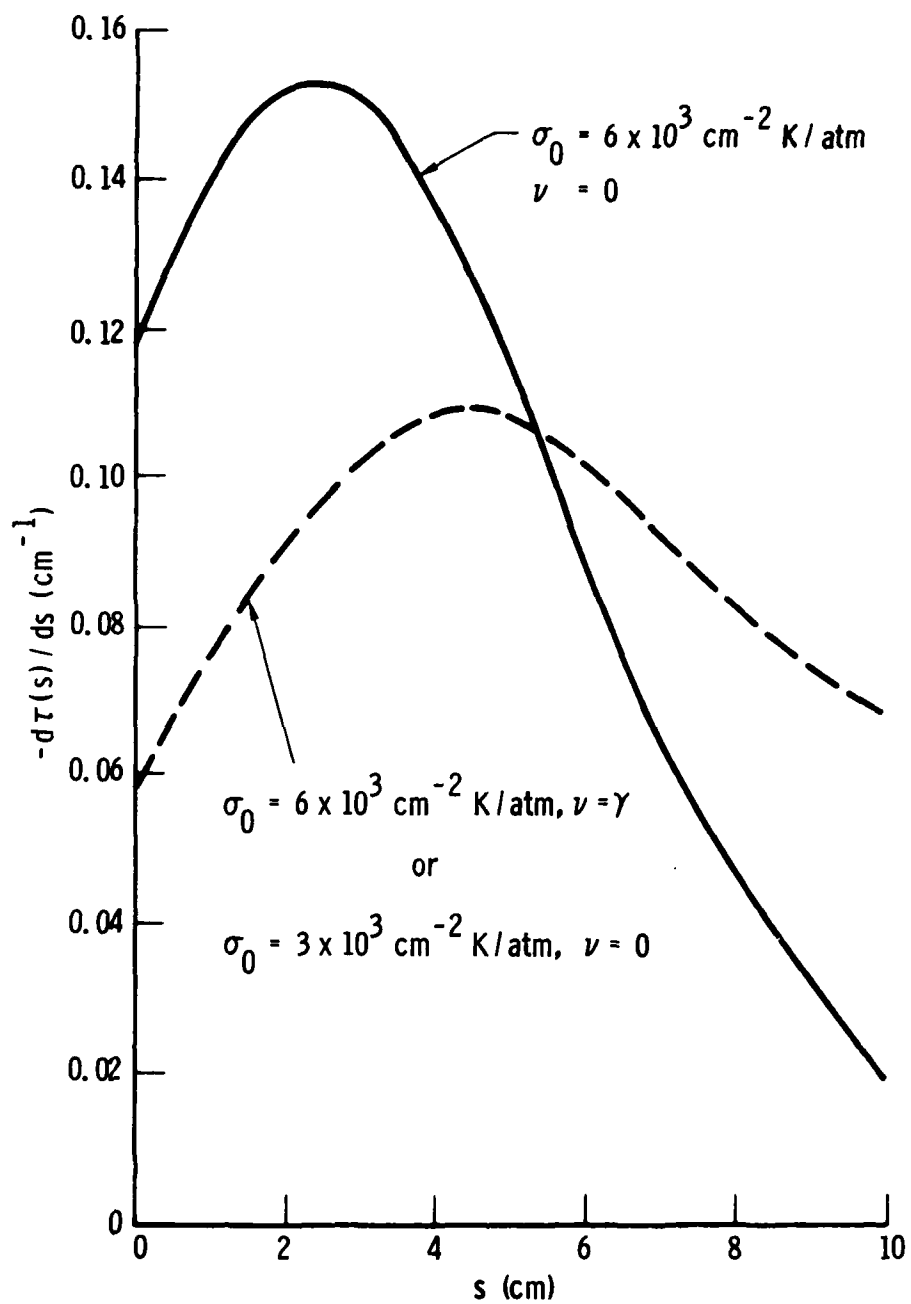


Fig. 30. Monochromatic weighting function for molecular infrared line.

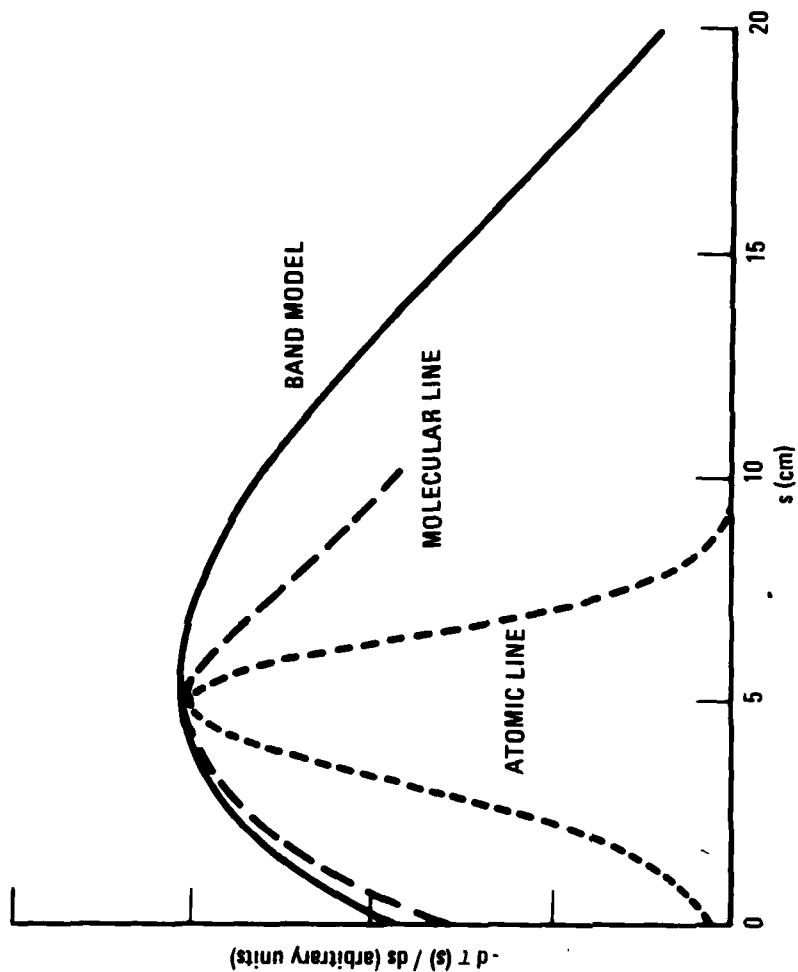


Fig. 31. Comparisons among band model, molecular line and atomic line weighting function.

between the isolated line curve that peaks at $s \approx 4.5$ cm and the band model curve of Fig. 11 at $\lambda = 5.08 \mu\text{m}$. The isolated line curve was scaled to match the peak height of the band model curve. Although the isolated line peak is narrower, it is not sufficiently narrower in this case to be of much use.

The second feature, that is that the whole plume cannot be covered, is immediately evident from Fig. 30. The top curve was obtained for the strongest line in the $2 \rightarrow 1$ band, but the peak position is only at $s \approx 2.5$ cm. There is no stronger line that can make the peak closer to $s = 0$ (for the plume pTc conditions used). In order for the peak to occur at $s = 0$ at the line center, the intrinsic line strength function must be greater than or equal to (see Eqs. 34 and 35),

$$\sigma_o = \frac{\beta\pi}{c\rho} \left[\frac{\theta}{T_B} - 1 \right] e^{\theta/T_B} \quad (36)$$

A comparison between the σ_o required by this criterion and the σ_o actually available for three diatomic molecules is given in Table 7. In no case does the available strength meet the required strength. In addition, a tradeoff effect is predicted by the data of this table (and substantiated by analysis). Namely, as θ is increased in order to obtain sharper peaked weighting functions, less and less of the plume around $s = 0$ can be probed for a given σ_o .

These results indicate that monochromatic multicolor inversion using infrared molecular lines is also not a good diagnostic for BATES motor plumes.

Table 7. Required and Available Line Strengths for Three Molecular Species

Species	Vibrational Transition	$\theta(K)$	$\sigma_0(\text{cm}^{-2} \text{ K/atm})$	
			Available	Required
HCl	1 - 2	4000	3.0 (3)	6.2 (4)
HF	1 - 2	5500	1.2 (4)	5.5 (5)
CO	1 - 2	3200	6.3 (3)	1.8 (4)

4.3 Application to Atomic Lines

This application to atomic lines considers atomic sodium as the diagnostic seed and observation of the visible lines that arise between the $3^2P_{1/2, 3/2}$ levels and higher energy levels. The $3^2P_{1/2, 3/2}$ level energy is approximately 16964 cm^{-1} and corresponds to $\theta = 11790 \text{ K}$. This value is 2 to 4 times larger than those used in the molecular line analysis. Line strength and position data for four doublet transitions are given in Table 8. For the strongest line listed, σ_0 is seen to be many orders of magnitude stronger than the largest line strength employed in the molecular line analysis.

The significant increase in θ and line strength for atomic lines provides for very much narrower weighting functions than for molecular lines. Consider the nominal BATES motor conditions $R(\text{radius}) = 10 \text{ cm}$, $p = 1 \text{ atm}$, $T_B = 800 \text{ K}$ and $\beta = 70 \text{ K/cm}$ ($T_0 = 1500 \text{ K}$). The weighting functions that peak at $s/R = 0.5$ and 0.3 are shown in Figs. 32 and 31, respectively. These functions are determined as follows: (1) the temperature at the desired position is calculated, (2) this temperature is used in Eq. 35 to get x_0 , and (3) x_0 is used in Eq. 31 to get the weighting function. The weighting function that peaks at 0.5 (Fig. 32) is compared with weighting functions derived previously within the band model formulation and for molecular lines. The atomic line function is significantly narrower than either of these functions. The faster rise is caused by the increased value of θ , and the faster fall is caused by the increased line strength.

Table 8. Atomic Sodium Line Data

$\lambda(\text{\AA})$	U	L	$\sigma_0(\text{cm}^{-2} \text{ K/atm})$
5149.09	$6^2S_{1/2}$	$3^2P_{1/2}$	4.9 (8)
5153.64		$3^2P_{3/2}$	9.8 (8)
5682.66	4^2D	$3^2P_{1/2}$	2.8 (9)
5688.22		$3^2P_{3/2}$	5.7 (9)
6154.23	$5^2S_{1/2}$	$3^2P_{1/2}$	1.0 (9)
6160.76		$3^2P_{3/2}$	2.1 (9)
8183.27	3^2D	$3^2P_{1/2}$	2.9 (10)
8194.81		$3^2P_{3/2}$	5.7 (10)

Line pair separation $\sim 17 \text{ cm}^{-1}$

Lower level energy $\sim 16964 \text{ cm}^{-1}$ ($\theta \approx 11790 \text{ K}$)

Line widths $\sim 0.1 \text{ cm}^{-1}/\text{atm}$

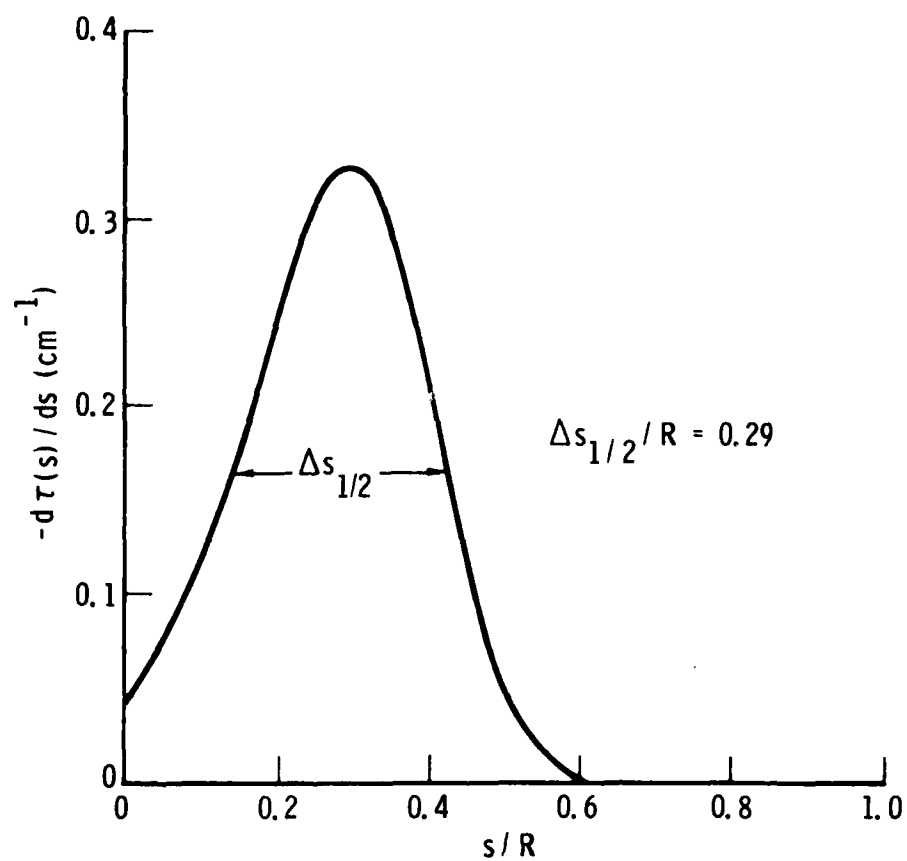


Fig. 32. Sodium line monochromatic weighting function that peaks at $s/R = 0.3$.

The criterion that has been used in previous analyses for determining whether or not a weighting function is narrow enough for accurate inversion is that the relative halfwidth $\Delta s_{1/2}/R$ of the weighting function that peaks at $s/R = 0.3$ be near the Cutting and Stewart value of $\Delta s_{1/2}/R \approx 0.3$. None of the temperature or plume size variations carried out in previous work was able to approach this value. The result shown in Fig. 31 indicates that monochromatic atomic line emission/absorption analysis could achieve this value.

This result is the first to indicate that multispectral emission/absorption diagnosis might work on plumes as small as and with as weak temperature dependences as the BATES motors. At least the first hurdle of being able to achieve narrow enough weighting functions has been overcome. Unfortunately, there are enough other objections to throw the scheme into disrepute. The most serious of these is the experimental resolution required to ensure the assumption of monochromaticity. As for molecular lines, the pressure broadening line parameter is of order 0.1 cm^{-1} at $p = 1 \text{ atm}$. A spectral resolution, then, of order 0.01 cm^{-1} (0.0036 \AA at 6000 \AA) would be desirable. Even if this resolution could be obtained, there are other serious problems with this diagnostic.

In Section 3.3.2, variations were made in the plume size to see if increased absorption (by increasing plume size) could lead to narrower weighting functions. It was found that it could, but that as a consequence, the degree of transmittance through the plume became immeasurably small. In effect, only the radiance profile was measurable, and only a temperature

profile could be retrieved. No information could be got on the concentration profile (and, in fact, a concentration profile had to be assumed in order to get the temperature profile). This same problem occurs in the monochromatic atomic line case, but to a much higher degree. For the two weighting functions that peak at 0.3 and 0.5, respectively, the x_0 values are 6.24×10^5 and 1.31×10^5 . The monochromatic transmittances through the whole plume for these values are $\tau = 2.0 \times 10^{-48}$ and 9.7×10^{-11} , again respectively. Thus the monochromatic atomic line method allows for a temperature profile determination only, and the sodium profile has to be known a priori. Assume that we desire only the temperature profile so that we can go on to more objections.

Sodium was selected because it is already a plume constituent at, nominally, ~ 40 ppm. This small concentration is not nearly large enough to achieve the peaking criterion of Eq. 35. For the weighting function that peaks at 0.3, for example, we require $x_0 = 6.24 \times 10^5$, which, from Eq. 34 we can deduce that we need a concentration of $c \sim 0.001$ if we use the second strongest line of Table 8 (i. e., $\sigma_0 = 2.9 \times 10^{10} \text{ cm}^{-2} \text{ K/atm}$). This is the concentration of free sodium that would be required. Being highly reactive, it seems sure at the relatively moderate temperatures of the BATES motors, that if additional sodium were needed in the plume, enough might have to be added to first chemically reduce all of the HCl and H_2O of the plume and then leave 0.1% mole fraction of free sodium left over. This could require a substantial amount of sodium and could surely be a serious perturbation of the normal plume conditions.

A final objection is that the degree of plume coverage is small. That is, the positions of the peaks of the weighting functions cannot be made to span the entire region $0 \leq s \leq R$. As in previous work, assume that we desire to span from $s/R = 0.1$ to $s/R = 0.9$. If we select $c = 0.0037$, then we force the strongest line of Table 8 to peak at 0.1. For this same concentration, however, the weakest line of Table 8 peaks at only $s/R = 0.69$. Thus the whole region is not covered. This flaw could be readily fixed by selecting one more lines, either weaker or stronger by a factor of ~ 3 than the weakest or strongest line, respectively, of Table 8.

4.4 Integrated Line Treatment for Atomic Lines

A significant problem with the monochromatic atomic line diagnostic scheme is the high spectral resolution requirement. On the other hand, the measurement of line radiance and absorptance integrated over the whole line is a relatively easy measurement. Much coarser spectral resolution can be employed, and although the observed line profile is seriously distorted by a wide slit, it is a well-known result that the area under the measured profile is the true integrated value regardless of the experimental resolution.

A slight problem might arise with sodium because of the doublet nature of the line array. It may be necessary to measure and work with the integrated effects of pairs of lines. Consider an isolated line. The integrated line radiance is given by Eqs. (1) and (3) as

$$N = \int_0^{\infty} B(s) \frac{dW(s)}{ds} ds \quad (37)$$

where $W(s)$ is the integrated absorptance (or, equivalent width) of the line for the optical path between $s = 0$ and general position s . The weighting function in this application is

$$g(s) = \frac{dW(s)}{ds}, \quad (38)$$

For a Lorentzian line and the linear temperature profile used so far, the following results can be obtained

$$W(s) = 2\pi\gamma L[\chi(s)], \quad (39)$$

$$\chi(s) = \chi_0 \left\{ E_1\left(\frac{\theta}{T(s)}\right) - E_1\left(\frac{\theta}{T_B}\right) \right\} s \leq R, \quad (40)$$

and

$$\frac{dW(s)}{ds} = \frac{2\pi\gamma\beta\chi_0}{\theta} \frac{\theta}{T_B} e^{-\theta/T(s)} \left\{ e^{-\chi(s)} I_0[\chi(s)] \right\} \quad (41)$$

where $L(\chi)$ is the Ladenburg-Reiche function

$$L(\chi) = \chi e^{-\chi} [I_0(\chi) + I_1(\chi)] \quad (42)$$

and $I_0(\chi)$ and $I_1(\chi)$ are modified Bessel functions. The similarity between the weighting function (Eq. 41) for this application and that Eqs. 31 and 32 for the monochromatic case is evident. Up to the term in brackets, the two equations (except for a constant $\pi\gamma$) are the same. The difference between

the two occurs only in the "transmittance" term in brackets. For the monochromatic case, this is $e^{-2\chi}$ while for the integrated line case it is $e^{-\chi} I_0(\chi)$. Both functions decrease with increasing χ (as is at least necessary in order for a peak to be formed in g). But, there is a significant difference; the monochromatic function falls sufficiently fast enough to form a narrow, well-defined peak whereas the integrated line function does not. While the monochromatic function continues to fall as $e^{-2\chi}$ as χ becomes large, the asymptotic limit of the integrated line function falls at the much slower rate of $1/(2\pi\chi)^{1/2}$. This slow fall-off cannot compete with the increase in g caused by the $e^{-\theta/T}$ term (at least, not until $T \sim \theta$).

The reason behind this anomalous behavior is as follows. Suppose we choose a value of concentration that causes the monochromatic weighting function evaluated at the line center to peak at some desired s/R . Then, in the line wings, the monochromatic weighting function would peak at a greater value of s/R (because the spectral absorption coefficient is less in the wings and c is constant). The farther out in the wing we go, the greater the value of s/R where the monochromatic weighting function peaks. The integrated effect of the whole line wing is to push the peak of the line weighting function all the way to $s = R$, that is, to the plume centerline. The final result is that the integrated line weighting functions are very broad and peak at $s \sim R$ regardless of the strength of the line.

5. SUMMARY AND CONCLUSIONS

The success of multispectral inversion rests on the existence of a set of weighting functions $g(s, \lambda)$ and the requirement that, as λ is varied, $s_p(\lambda)$ spans the range of optical path over which information is desired. The sharp peaking ensures that the measured E/A characteristics at λ reflect conditions in a small region about $s_p(\lambda)$. The narrower the weighting functions, the greater the spatial resolution of the inversion. Within a given spectral scale (e.g. monochromatic or band model) the shapes of the weighting functions are determined almost exclusively by the properties of the gas medium and very little by the mathematical method of inversion.

In all multispectral applications, the peaking of the weighting function is caused by an interplay between an increasing and decreasing function of s written as a product. In plume applications, the increasing function is the line strength S (monochromatic application) or the absorption band model parameter \bar{k} (band model application), and the decreasing function is the transmittance between $s = 0$ (sensor position) and general position s . Inasmuch as S and \bar{k} are generally increasing functions of temperature in the temperature regime of tactical motor plumes, a peaked weighting function requires a temperature increase with s . For an observation line of sight that runs from plume boundary-to-plume center-to plume boundary, this requirement limits the application to plumes (assumed to be cylindrically symmetric) whose temperature falls monotonically between the plume axis and plume boundary and also limits the probing region to one-half the plume diameter. The sharpness

of the weighting functions is determined principally by the degree of temperature gradient along the line of sight. The larger the temperature gradient, the sharper the rise. The sharpness of the trailing edge is determined by the strength of absorption. The larger the optical depth of the plume, the faster the rate of fall-off of the trailing edge.

The main conclusion drawn from the work reported here is that for either band model or monochromatic (line center) applications in the infrared, the relatively mild temperature gradients and small optical depths encountered in typical tactical motor plumes yield weighting functions that are not narrow enough to effect acceptable inversion results. For the test case chosen (parabolic temperature profile with $T_o = 1500$ K, $T_B = 750$ K, $R = 10$ cm, $p = 1$ atm, $c = 0.15$) and in the optimum spectral region ($4.3\text{-}\mu\text{m}$ CO_2 red wing), the retrieved temperature profile was roughly parabolic with $T_o = 1360$ K and $T_B = 1050$ K). The errors at plume center and boundary were -9 and +40 percent, respectively. The retrieved concentration was low by 27 percent. No significant improvements results for likely extremes of size and temperature gradient in tactical motor plumes. Given that these results were obtained in the best available infrared region (and which might not even be available in practice because of CO contamination) and because this example does not consider the severe degradation of inversion caused by account of random experimental errors, the conclusion of unacceptability is well founded.

Atomic lines yield much sharper monochromatic weighting functions than do molecular lines. This results from the fact that the lower energy

levels of the probing lines are substantially higher than those for the molecular lines (yielding a more sensitive response to temperature changes) and because the intrinsic line strengths of atoms are orders of magnitude stronger than for molecules (giving a sharper fall off). The example employing sodium lines gave weighting functions that are as narrow as those obtained in the furnace work of Cutting and Stewart and would yield a temperature inversion of comparable accuracy (a few percent with $\sim 0.2 R$ spatial resolution). The most serious defect of the method is the extremely high resolution required to obtain E/A data at the line centers. It is estimated that an experimental resolution of near 0.004 \AA at 6000 \AA would be required. Additionally, at least for sodium, chemical reactivity with other plume constituents would require a substantial seeding fraction (up to 30%) so that the plume would be severely perturbed. In principle, some nonreactive seeding atom might be found to obviate this objection. However, even then, one final objection remains; the optical depth is so large that the line center transmittance through the plume is unmeasurable. Thus, the seeding concentration cannot be measured optically and would have to be independently measured even in order to obtain the temperature profile. Also, of course, no information whatsoever on molecular concentrations is available with the atomic line method. In total, multispectral inversion using atomic lines does not appear to be immediately practical.